

This is an Open Access document downloaded from ORCA, Cardiff University's institutional repository: <https://orca.cardiff.ac.uk/id/eprint/113588/>

This is the author's version of a work that was submitted to / accepted for publication.

Citation for final published version:

Masum, Shakil A. and Thomas, Hywel R. 2018. Modelling coupled microbial processes in the subsurface: model development, verification, evaluation and application. *Advances in Water Resources* 116 , pp. 1-17.
10.1016/j.advwatres.2018.03.015

Publishers page: <https://doi.org/10.1016/j.advwatres.2018.03.015>

Please note:

Changes made as a result of publishing processes such as copy-editing, formatting and page numbers may not be reflected in this version. For the definitive version of this publication, please refer to the published source. You are advised to consult the publisher's version if you wish to cite this paper.

This version is being made available in accordance with publisher policies. See <http://orca.cf.ac.uk/policies.html> for usage policies. Copyright and moral rights for publications made available in ORCA are retained by the copyright holders.



38 Microbial activities have adverse or unwanted impacts on public health, ground engineering works etc.,
39 but they can be adopted to a wide range useful applications. For example, biofilms are used as bio-
40 barriers. They can also be used for bioremediation of pollutant plumes or to enhance oil recovery (Chen-
41 Charpentier, 1999). They facilitate biotransformation, a process by which toxic pollutants are
42 transformed into non-toxic substances (Cunningham et al., 1991; Chen-Charpentier, 1999). With regard
43 to Carbon Capture and Sequestration (CCS) technologies, subsurface biofilms have been found
44 effective in enhancing CO₂ trapping mechanisms and limiting the leakage of sequestered supercritical
45 carbon dioxide through geologic cap-rocks, formation fractures and near the injection wells (Mitchell
46 et al., 2009). Therefore, to ensure their effective usages, understanding of the fundamental processes in
47 porous media is essential.

48

49 In saturated porous media, microbial processes and their impacts on physical properties of the media
50 have been studied extensively via laboratory experiments (Trulear and Characklis, 1980; Bakke, 1986;
51 Taylor and Jaffe, 1990a; Cunningham et al., 1991; Vandevivere and Baveye, 1992a, b; Baveye et al.,
52 1992; Seki et al., 1998; Ginn et al., 2002; Mitchell et al., 2009 and others) and by using theoretical and
53 numerical methods (Rittmann and McCarty, 1980; Corapcioglu and Haridas, 1984, 1985; Bakke, 1986;
54 Taylor et al., 1990; Taylor and Jaffe, 1990b, c; Rittmann, 1993; Chen-Charpentier, 1999; Murphy and
55 Ginn, 2000; Seki and Miyazaki, 2001; Thullner and Baveye, 2008 and others). In contrast, limited
56 attempts have been made to explore the processes in unsaturated conditions (Schaefer et al., 1998;
57 Rockhold et al., 2004; Yarwood et al., 2006; Maggie and Porporato, 2007; Mostafa and van Geel, 2007;
58 Gargiulo et al., 2007; Ebigbo et al., 2010; Rosenzweig et al., 2013, 2014).

59

60 Microbial cells in the suspended or planktonic state, in saturated or nearly-saturated porous media, are
61 transported via physicochemical processes such as convection, dispersion, diffusion, straining and
62 filtration (Murphy and Ginn, 2000; Ginn et al., 2002). However, in unsaturated conditions, the concept
63 of planktonic free movement is unlikely and microbes predominantly exist as biofilms at the solid
64 surfaces (Or et al., 2007). In saturated conditions, the dominant microbial life is also in biofilms. To
65 assess the impacts of microbial activities in such conditions, it is important to understand the factors
66 influencing the transport and reaction mechanisms as well as the quantity of biomass in the medium.
67 Net accumulation of biofilms and suspended cells depends on growth and decay rates controlled by
68 various physical and chemical processes. Cunningham et al. (1991) reported from Escher (1986) that
69 under constant supply of growth nutrients, sorption related processes are controlled by suspended cell
70 concentrations and growth processes at solid surfaces are regulated by the concentrations of attached
71 microbes on those surfaces. In deep subsurface environments or in absence of a suitable external
72 electron acceptor, bacteria reproduce primarily by metabolising growth substrates or fermentation;
73 however in presence of electron acceptors they grow by respiration (Bethke, 2008). Microbial
74 population reduces due to cell death as well as in presence of biocides. Biocide, such as supercritical

75 CO₂, reduces the number of living cells in the liquid phase (Zhang et al., 2006). The movement of
76 microbes between the planktonic state and sessile state also affects biomass quantity in individual
77 phases. For example, biofilm mass loss due to high liquid shear force at the biofilm-liquid interface
78 (Trulear and Characklis, 1980; Rittmann, 1982; Bakke, 1986) or due to changes in physiochemical
79 conditions (Bakke, 1986); results in an increase of suspended microbes in the liquid phase. In addition,
80 attachment and detachment of cells may take place to and from biofilm phase (Cunningham et al.,
81 1991), until a steady-state is reached between suspended cell and biofilm concentrations. Microbial
82 processes are also affected by the chemical constituents of the medium (Or et al., 2007). Reactive
83 transport and supply of growth nutrients might be affected by the presence of various chemicals and
84 minerals. Conversely microbes promote certain reactions that alter the local geochemical condition of
85 the native media. Microbial growth kinetics are influenced by pH of the system (Ibragimova et al., 1969;
86 Tan et al., 1998; Hořtacká et al., 2010; Rousk et al., 2009). In their experiments, Hořtacká et al. (2010)
87 observed significant growth at pH 8.5 than in pH less than 6.0. As the pH of a system changes, ionization
88 states of the components in the system also changes (Dixon and Webb, 1979). The active components
89 of microbial cells are usually the cell-enzymes (Tan et al., 1998). Enzymes contain ionizable groups
90 which need to be in appropriate ionic states to bind substrates, catalyzes reactions, and to produce
91 biomass (Segel, 1975). The study of such complex coupled interactions in variably saturated porous
92 media is challenging and rarely available in literatures.

93
94 In the scope of this study, a microbial model has been developed at the macroscale of a porous medium
95 within a coupled thermal-hydraulic-chemical-mechanical (THCM) framework. The aim of the research
96 is to analyse the impacts of microbial processes on physical and chemical behaviours of the medium
97 which subjected to simultaneous flow, reaction and deformation conditions. The THCM model,
98 COMPASS (Thomas and He, 1998; Seetharam et al., 2007; Masum, 2012; Sedighi et al., 2015), is based
99 on a mechanistic approach in which the mechanisms to explain relevant behaviours are included in an
100 additive manner with inter-related couplings as required. COMPASS is linked with the geochemical
101 model PHREEQC version 2.0 (Parkhurst and Appelo, 1999) which estimates both thermodynamically
102 equilibrium and kinetically controlled chemical reactions. The advanced modelling capabilities have
103 been exploited to investigate the aforementioned complex microbial processes in the subsurface soils.

104
105 In this paper, theoretical and numerical developments of the microbial model including the couplings
106 between transport module and reaction module are presented. Verifications of the model and
107 evaluations against experimental results have been conducted. The model has been applied to predict
108 biofilm growth in a variably saturated sandstone core and under changing pH condition. The model is
109 then used to investigate microbial respiration in a coupled two-phase flow condition. Finally, a
110 simulation of microbial growth via fermentation has been demonstrated. Since microbes in unsaturated
111 condition mainly exist by forming biofilms, model simulations and applications presented here are

112 focused on the biofilm processes only. The feedback of net biomass accumulation on media porosity,
 113 permeability is estimated through a mass-volume relationship. In this article, biofilms are assumed to
 114 be impermeable and water inside the biofilm is immobile and concentration of substrate in the biofilm
 115 is the same as in the liquid phase. In the simulations, it has been considered that the biofilm reached to
 116 mature state (Bakke, 1986) during the settlement period and its density remains constant throughout
 117 the simulation. That means that although the biofilm mass grows (or reduces) during the simulation, the
 118 ratio between bacterial cell mass and biofilm (cell+EPS) mass remains unchanged (at the early stages
 119 of biofilm development the ratio varies with time). The model is presented here for isothermal
 120 conditions and mechanical stress/ strain is ignored. Microbial processes including suspended cells,
 121 thermal gradients and mechanical deformation will be addressed in future publications.

122

123 **2. The Model**

124 The nomenclature is presented in Table A of Appendix A.

125

126 *2.1 Theoretical formulation*

127 In an unsaturated porous medium that contains microbial biofilm, the total porosity (n_0) can be divided
 128 into liquid phase, gas phase and biofilm phase as,

$$\theta_l + \theta_g + \theta_b = n_0 \quad (1)$$

129 where θ_l , θ_g , θ_b are the volumetric liquid, gas and biofilm contents, respectively. Growing biofilms
 130 occupy inter-particle spaces and restrict the overall flow processes in the medium. Therefore, porosity
 131 is affected by the volume of biofilm phase and,

$$\theta_l + \theta_g = n_0 - \theta_b = n. \quad (2)$$

132 Here n is the active porosity that is unaffected by the biofilm phase and where flow of fluids primarily
 133 takes place. By expressing the volumetric liquid content $\theta_l = nS_l$ and the volumetric gas content $\theta_g =$
 134 nS_g ; the relationship between liquid saturation (S_l) and gas saturation (S_g) yields, $S_g + S_l = 1$. It has
 135 been considered that the gas phase is unsuitable for the survival of microbes, as a result, the spread of
 136 attached biomass in the solid phases should be encapsulated within the liquid phase volume of the
 137 media. Following Effendiev (2013), it has been assumed that growing biofilm assimilates the liquid
 138 phase rather than pushing it out of the system.

139

140 *2.1.1 Conservation of microbial biomass*

141 The mass conservation equation of a suspended cell in the liquid phase is expressed as,

$$\frac{\partial}{\partial t}(\theta_l c_b^l) = \nabla(\theta_l D_b^* \nabla c_b^l) + \nabla(\theta_l v_l c_b^l) + s_b^l \quad (3)$$

142 where c_b^l is the concentration of the suspended microbe and D_b^* is the hydrodynamic dispersion
 143 coefficient in the liquid phase. Details of hydrodynamic dispersion in the model is presented in Section
 144 2.1.5. v_l represents velocity of the liquid phase and s_b^l represents the sinks or sources.

145

146 The mass balance equation of a biofilm attached to solid surfaces is given by,

$$\frac{\partial}{\partial t}(c_b^s) = s_b^s \quad (4)$$

147 where c_b^s is the amount of biofilm per unit volume of the porous media and s_b^s represents the sinks or
 148 source terms. Biofilm concentration (c_b^s) is related to biofilm volumetric content via $c_b^s = \theta_b \rho_b^s$, where
 149 ρ_b^s is the biofilm mass density *i.e.* the amount of dry biomass per unit wet volume of the biofilm.

150

151 Microbial sinks/ sources include physical growth (*e.g.* substrate metabolism, attachment) and decay
 152 processes (*e.g.* endogenous decay, biocide decay, detachment, shear loss etc.), local geochemical
 153 condition (r_{chem}) and the presence of external sinks or sources (r_{ext}). Therefore,

$$S_b^i = r_\alpha - r_\beta \pm r_{chem} \pm r_{ext} \quad i \in \{l, s\} \quad (5)$$

154 where α represents the growth rates and β represents the decay rates. Superscript l and s represents
 155 suspended biomass and attached biofilm, respectively.

156

157 Subsurface microbes primarily grow by metabolising growth-limiting substrates. If growth is limited
 158 by both a substrate and an electron acceptor, then the process is explained by the dual Monod's kinetics
 159 as follows:

$$r_{substrate} = k_+ \left(\frac{c_d^s}{K_s' + c_d^s} \right) \left(\frac{c_d^e}{K_e' + c_d^e} \right) \theta_l c_b^l \quad [\text{suspended biomass}] \quad (6a)$$

$$r_{substrate} = k_+ \left(\frac{c_d^s}{K_s' + c_d^s} \right) \left(\frac{c_d^e}{K_e' + c_d^e} \right) c_b^s \quad [\text{attached biofilm}]. \quad (6b)$$

160 Here k_+ is the substrate utilisation rate. c_d^s is the substrate concentration and c_d^e is the concentration of
 161 electron acceptor in the liquid phase. K_s' and K_e' are Monod half-saturation constants of substrate and
 162 electron acceptor, respectively.

163

164 Biomass decay is expressed using a first-order rate as follows:

$$r_{decay} = k_- \theta_l c_b^l \quad [\text{suspended biomass}] \quad (7a)$$

$$r_{decay} = k_- c_b^s \quad [\text{attached biofilm}]. \quad (7b)$$

165 Here k_- is a combined decay rate that includes both endogenous and biocide-induced death.

$$k_- = k_-^e + k_-^b \quad (8a)$$

166 where k_-^e is the endogenous death rate and k_-^b is the biocide mediated reduction rate, which accounts
 167 microbial death due to a toxic non-wetting phase such as scCO₂, and mass transfer of high

168 concentrations of CO₂ into the aqueous phase. Biocide decay rate as a function of gas phase saturation
 169 has been suggested by Ebigbo et al. (2010).

$$k_-^b = c_-^b (S_g)^{c_c} \quad (8b)$$

170 where c_-^b and c_c are empirical parameters depending on the bacterial species/ biofilm and on the porous
 171 media properties.

172

173 Loss of biomass from biofilms might occur due to fluid shear stress. Bakke (1986) observed removal
 174 of small particles from biofilms at the biofilm-liquid interface due to the shear stress imposed by the
 175 flowing liquid. Following Bakke (1986) biofilm shear loss is written by,

$$r_{shear} = b_s c_b^s \quad (9)$$

176 where b_s is the detachment rate due to liquid shear stress τ . The relationship between τ and b_s can be
 177 expressed as, $b_s = k_\tau \tau$. Here k_τ is a specific shear loss coefficient. For Newtonian liquids, shear stress
 178 (τ) can be obtained from dynamic viscosity (μ_l) and velocity gradient. Therefore,

$$\tau = \mu_l \nabla v_l \quad (10)$$

179 Concentration of suspended cells in the liquid phase is increased by shear loss of biofilms. Meanwhile,
 180 attachment of suspended cells from liquid phase to biofilms reduces the amount in suspension. These
 181 processes are expressed using a linear first-order relationship.

$$r_{attachment/detachment} = k_a \theta_l c_b^l - k_d c_b^s \quad (11)$$

182 where k_a and k_d are the attachment and detachment rates of cells to and from the biofilms respectively.
 183

184 Impacts of local geochemical environment on microbial activities are estimated by the r_{chem} term in
 185 the model. Concentrations of dissolved chemicals and minerals, redox state, pH etc. are calculated/
 186 updated from bio-geochemical reactions via the geochemical model. The information is then used to
 187 predict microbial physical processes implemented in the transport model and vice-versa. For example,
 188 dissolution of CO₂ in porewater reduces the pH of the system (which is evaluated by the chemical
 189 model) and the effect of pH on microbial growth can be estimated from the transport model. Ibragimova
 190 et al. (1969) and Tang et al. (1989) proposed a pH dependent growth kinetic,

$$k_{pH} = \frac{k_0^p K_1^p}{K_1^p + [H^+]}. \quad (12)$$

191 Here k_{pH} is a pH-dependent growth rate. k_0^p is a specific growth rate with respect to pH which
 192 determines the shape of the k_{pH} -pH diagram. K_1^p is an empirical constant, known as ionisation constant
 193 (Tan et al., 1998) and $[H^+]$ represents the concentration of hydrogen ion (mol/L) in the liquid solution.
 194 Figure B1 (Appendix B) shows the behaviour of k_{pH} as a function pH for different values of k_0^p and
 195 K_1^p . The pH-dependent microbial growth can be expressed as,

$$r_{chem} = k_{pH} \theta_l c_b^l \quad [\text{suspended biomass}] \quad (13a)$$

$$r_{chem} = k_{pH}c_b^s \quad [\text{attached biofilm}]. \quad (13b)$$

196 Since solution pH influences substrate binding with microbial cells, pH-dependent growth rate is linked
 197 with that of the substrate utilisation, *i.e.* Equation (6). In absence of a growth substrate, solution pH
 198 alone does not influence microbial growth. In a similar manner, the effects of other chemical processes
 199 on the net microbial growths can be included. Implementations of the microbial processes within the
 200 THCM model and the linkage with the geochemical model are described in section 2.2.

201

202 2.1.2 Conservation of dissolved chemicals

203 The governing equation of multicomponent chemical flow in a liquid phase is given by,

$$\frac{\partial(\theta_l c_d^i)}{\partial t} = \nabla(\theta_l D_d^* \nabla c_d^i) + \nabla(\theta_l c_d^i v_l) + s_d^i \quad (14)$$

204 where c_d^i represents the concentration and D_d^* is the hydrodynamic dispersion coefficient (Section
 205 2.1.5) of the i^{th} component in the liquid phase. S_d^i represents the total sink/ source for the i^{th} component
 206 including geochemical reactions, microbial interactions and any external source or sink. Microbial
 207 growth reduces the amount of substrate and electron acceptor (*i.e.* dissolved oxygen) and their
 208 respective sinks s_d^s, s_d^e can be expressed as,

$$s_d^s = -r_{substrate}/Y \quad (15a)$$

$$s_d^e = -F r_{substrate}/Y \quad (15b)$$

209 where Y is the growth yield *i.e.* the amount of biomass created per unit mole of substrate (Bethke, 2008)
 210 and F is the oxidiser yield which represents the amount of oxygen consumed per unit mass of substrate
 211 (Murphy and Ginn, 2000). Please note in Equation (6) $i = s$ denotes the presence of a single growth
 212 substrate.

213

214 2.1.3 Conservation of liquid and gas

215 The mass conservation equation for the liquid phase flow is expressed as,

$$\frac{\partial(\theta_l \rho_l)}{\partial t} = \nabla(\rho_l v_l) + S_s \quad (16)$$

216 where, ρ_l is the liquid density which is constant in this study and S_s represents the liquid phase sink/
 217 source. Liquid velocity (v_l) is calculated using the Darcy's law,

$$v_l = -\frac{K_{int} k_{rl}}{\mu_l} \nabla u_l. \quad (17)$$

218 Here u_l denotes the porewater pressure, k_{int} is the in-situ intrinsic permeability, k_{rl} is the liquid phase
 219 relative permeability.

220

221 The multicomponent gas transport equation is given by,

$$\frac{\partial(\theta_g c_g^i)}{\partial t} = \nabla(\theta_g D_g^i \nabla c_g^i) + \nabla(\theta_g c_g^i v_g) + s_g^i. \quad (18)$$

222 Here c_g^i is the concentration and D_g^i is the effective diffusion coefficient of the i^{th} gas species. Since,
 223 gas phase molecular diffusion often dominates mechanical dispersion (Costanza-Robinson and
 224 Brusseau, 2006), effective diffusion coefficient of i^{th} species is calculated as,

$$D_g^i = \tau_g D_g^0. \quad (19a)$$

225 Here D_g^0 is the molecular diffusion coefficient of gas in free flow condition. In a mixture of gases
 226 diffusion of one component may be affected by the others. Estimation of multicomponent molecular
 227 diffusion coefficients in the model is based on the method (Generalized Multicomponent Fick's Law)
 228 proposed by Taylor and Krishna (1993) and has been presented elsewhere (Masum et al., 2012; Masum,
 229 2012). However, multi-nary interactions among gas components have been ignored in this paper and
 230 only self-molecular-diffusion of components has been considered. τ_g in Equation (19a) is the gas phase
 231 tortuosity factor, which is obtained from the Millington and Quirk (1961) model as,

$$\tau_g = n^{1/3} S_g^{7/3}. \quad (19b)$$

232 The sink/ source term s_g^i includes gas phase reactions, dissolution (or formation) in the liquid phase and
 233 external sinks or sources of the i^{th} gas species. Partitioning of components between gas phase and liquid
 234 phase is considered to be in equilibrium following Henry's law. Gas components, which dissolve in
 235 liquid phase, are treated as dissolved chemicals (Equation 14) and therefore, the i^{th} component of s_g^i is
 236 linked with that of s_d^i via $c_d^i = H_c c_g^i$. Here, H_c is Henry's constant.

237

238 The gas phase velocity,

$$v_g = -\frac{K_{int} k_{rg}}{\mu_g} \nabla u_g \quad (20)$$

239 where k_{rg} is the gas phase relative permeability and μ_g is the dynamic viscosity of the gas phase. The
 240 total gas pressure (u_g) is obtained by using the ideal gas law.

$$u_g = \sum_{i=1}^{N_g} c_g^i RT \quad (21)$$

241 Here N_g is the total number of gas components, R is the universal gas constant and T is the reference
 242 temperature.

243

244 Original intrinsic permeability ($k_{int,0}$) of porous media, which is a function of material structure only,
 245 is affected by biofilm growth. The in-situ intrinsic permeability (k_{int}) is estimated from the original
 246 permeability using the expression given by Somerton et al. (1975).

$$\frac{K_{int}}{k_{int,0}} = \left(\frac{n}{n_0}\right)^3 \quad (22)$$

247

248

249 *2.1.4 Soil water characteristic behaviour and relative permeability*

250 In a multiphase system, the presence of both gas phase and liquid phase leads to matric suction (s)
 251 which is expressed as, $s = u_g - u_l$. Suction often regulates the saturation states of a porous medium
 252 and it is measured from water retention behaviours of the medium. In this paper, the water retention
 253 behaviour is based on the van Genuchten (1980) model.

$$S_l = S_r + (1 - S_r) \left[\frac{1}{1 + |\alpha h|^\beta} \right]^m \quad m = 1 - \frac{1}{\beta} \quad (23)$$

254 where α, m, β are curve fitting parameters, S_r is the residual degree of saturation and h is suction head
 255 ($= s/\gamma_l$). Here, γ_l is the unit weight of water.

256

257 The liquid phase relative permeability is defined by (van Genuchten, 1980),

$$k_{rl} = S_e^{1/2} \left(1 - (1 - S_e^{1/m})^m \right)^2 \quad (24)$$

258 Parker et al. (1987) presented the gas phase relative permeability,

$$k_{rg} = (1 - S_e)^{1/2} (1 - S_e^{1/m})^{2m}. \quad (25)$$

259 Here S_e denotes the effective saturation.

$$S_e = \frac{S_l - S_r}{1 - S_r} \quad (26)$$

260

261 *2.1.5 Hydrodynamic dispersion*

262 Hydrodynamic dispersion coefficient (Equation 3 & 14) includes both mechanical dispersion
 263 coefficient and effective molecular diffusion coefficient. Bear and Verruijt (1987) proposed
 264 hydrodynamic dispersion coefficient as,

$$D_d^* = D_d^h + D_d^i. \quad (27a)$$

265 Here D_d^h is the coefficient of mechanical dispersion and it is considered to be a function of the average
 266 fluid velocity (Pickens and Gillham, 1980). Hydrodynamic dispersion affects the spread of dissolved
 267 chemicals or suspended microbes both in parallel (longitudinal) and in perpendicular (transverse)
 268 directions to flow. In this paper, only longitudinal dispersion is considered. Therefore,

$$D_d^h = \alpha_L |v_l| \quad (27b)$$

269 where, α_L is the coefficient of longitudinal dispersivity and $|v_l|$ is the absolute average velocity of liquid
 270 phase.

271

272 The effective molecular diffusion coefficient of i^{th} chemical component is calculated as,

$$D_d^i = \tau_l D_d^0. \quad (28a)$$

273 Here D_d^0 is the molecular diffusion coefficient of chemical in free flow and τ_l is the porous media
 274 tortuosity factor in the liquid phase, which is obtained from the Millington and Quirk (1961) model as,

$$\tau_l = \theta_l^{7/3} / n^2. \quad (28b)$$

275

276 2.2 Numerical formulation

277 The microbial model has been developed within the THCM model, COMPASS (COde of Modelling
 278 PArtially Saturated Soils). The detailed developments of COMPASS including theoretical and
 279 numerical formulations, verifications, validations and numerous applications have been presented
 280 elsewhere (Thomas and He, 1998; Seetharam, 2003; Seetharam et al., 2007; Masum, 2012; Sedighi et
 281 al., 2015). In the model, the governing transport equations are expressed in terms of the primary
 282 variables, *i.e.* porewater pressure (u_l), poregas concentration (\mathbf{c}_g), dissolved chemical concentration
 283 (\mathbf{c}_d), suspended biomass concentration (\mathbf{c}_b^l), biofilm concentration (\mathbf{c}_b^s), temperature (T) and
 284 displacement (\mathbf{u}). For example, Equation (3) can be expressed in terms of primary variables as follows:

$$C_{c_b l} \frac{\partial u_l}{\partial t} + C_{c_b c_g} \frac{\partial c_g}{\partial t} + C_{c_b c_b} \frac{\partial c_b^l}{\partial t} + C_{c_b u} \frac{\partial \mathbf{u}}{\partial t} = \nabla(K_{c_b c_b} \nabla c_b^l) + \nabla(K_{c_b l} \nabla u_l) + s_b^l \quad (29)$$

285 where,

$$286 C_{c_b l} = -n c_b^l \frac{\partial S_l}{\partial S}, C_{c_b c_g} = -n R T c_b^l \frac{\partial S_l}{\partial S}, C_{c_b c_b} = n S_l, C_{c_b u} = S_l c_b^l W^T P, K_{c_b c_b} = \theta_l D_b^*, K_{c_b l} = \frac{K_{int} k_{r l}}{\mu_l}$$

287 Here P is the strain matrix and W is a vector of differential operators. Following that, the equations are
 288 spatially discretised using Galerkin Finite Element Method (GFEM). Please note that the 7th term (or
 289 microbial sinks/ sources) in Equation (29) is implemented in the model following a sequential non-
 290 iterative approach (SNIA). As per this approach, the sink/source is calculated only once in each time
 291 step after the convergence of the transport equations are achieved. Therefore, dropping this term, the
 292 approximated form of Equation (29) yields,

$$-C_{c_b l} \frac{\partial \hat{u}_l}{\partial t} - C_{c_b c_g} \frac{\partial \hat{c}_g}{\partial t} - C_{c_b c_b} \frac{\partial \hat{c}_b^l}{\partial t} - C_{c_b u} \frac{\partial \hat{\mathbf{u}}}{\partial t} + \nabla(K_{c_b c_b} \nabla \hat{c}_b^l) + \nabla(K_{c_b l} \nabla \hat{u}_l) = R_\Omega \quad (30)$$

293 Here R_Ω is the residual error imposed due to the approximation over the domain, Ω and $(\hat{\cdot})$ indicates
 294 the approximated primary variables. The aim of the Galerkin weighted residual method is to reduce the
 295 residual error to zero in some average sense over the domain. The matrix form of the governing
 296 equations, following the GFEM, can be expressed as follows:

$$\mathbf{A}\boldsymbol{\varphi} + \mathbf{B} \frac{d\boldsymbol{\varphi}}{dt} + \mathbf{C} = \{\mathbf{0}\} \quad (31)$$

297 where \mathbf{A} , \mathbf{B} , \mathbf{C} are the matrices of coefficients and $\boldsymbol{\varphi}$ is the vector of primary variables *i.e.*, $\boldsymbol{\varphi} =$
 298 $\{u_l, T, c_g^l, \dots, c_g^{N_g}, c_d^l, \dots, c_d^{N_d}, c_{b,i}^l, \dots, c_{b,N_b}^l, c_{b,i}^s, \dots, c_{b,N_b}^s, u\}$. Here, N_g , N_d , N_b^l and N_b^s are the total
 299 number of gas, dissolved chemicals, suspended biomass and biofilm species in the system respectively.
 300 An implicit mid-interval backward difference procedure is used for temporal discretisation of Equation
 301 (31). Finally, an iterative solution procedure called the predictor-corrector algorithm (Douglas and
 302 Jones, 1963) is applied to solve the set of equations. A schematic diagram (or flowchart) describing the
 303 coupled microbial processes in COMPASS and the linkage with PHREEQC is presented in Figure 1.

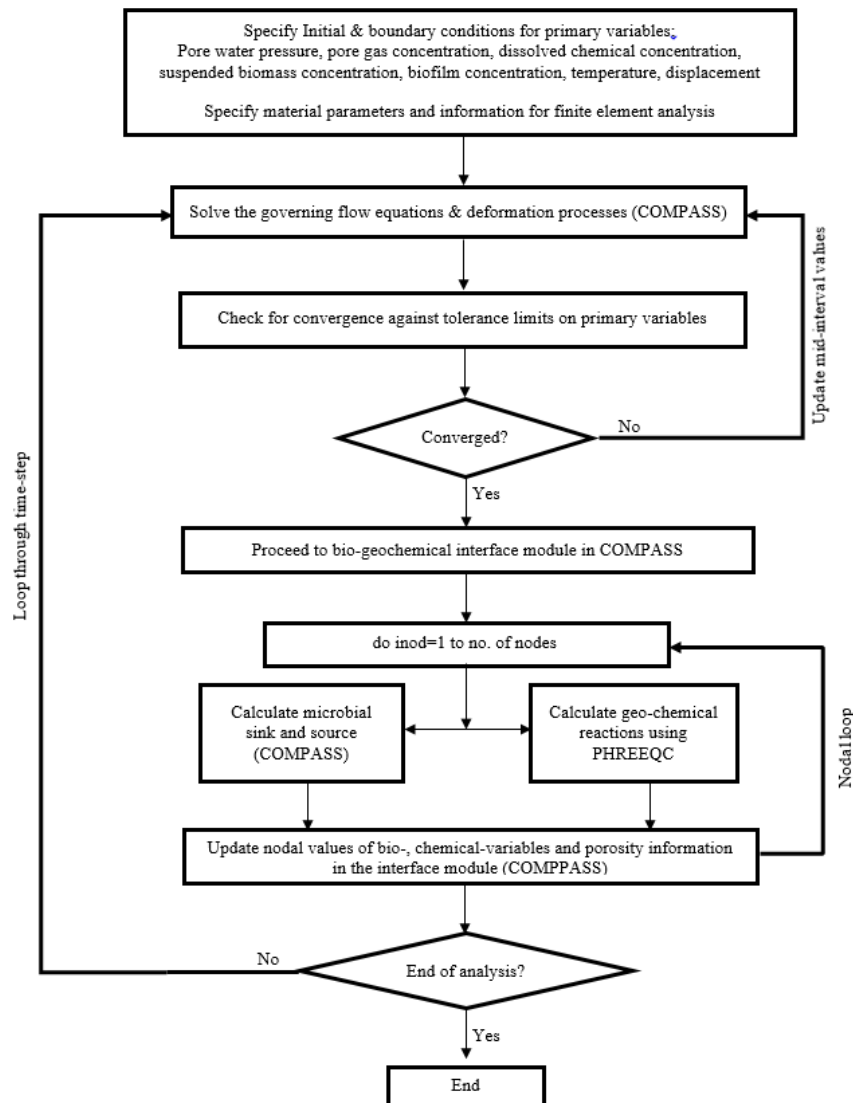


Figure 1 Flowchart diagram of the coupled microbial model. The transport model, COMPASS, is linked with geochemical reaction model, PHREEQC version 2.0. The microbial processes and geochemical reactions are linked via SNIA, since they are handled only once in every time step after the convergence of transport equations occurs.

305

306 COMPASS code has been developed on Fortran F90 while PHREEQC is available in C Programming
 307 language. The COMPASS-PHREEQC model runs on a combine Fortran-C platform. Once the
 308 convergence of primary variables (solving governing flow and deformation equations) is achieved, the
 309 programme proceeds to the bio-geochemical interface (in COMPASS) where microbial and
 310 geochemical reaction sink/ sources are estimated at every nodal points. Depending on the problem,
 311 either of the sink/ sources can be estimated first. For example, dissolution of CO₂ reduces pH of a
 312 system, which consequently affect microbial growth. In this case, geochemical reaction (in PHREEQC)
 313 is estimated initially and then the updated information is used to calculate microbial sink/ sources.

314 Concentrations of chemicals, minerals, gases and microbes (for microbial-induced mineral kinetics),
 315 from the bio-geochemical module, are passed to PHREEQC as input data. Simultaneously an input file,
 316 including relevant thermodynamic and kinetic reactions information, is also provided to proceed
 317 PHREEQC calculations. Following the measurements of microbial and geochemical reaction sink/
 318 sources, the primary variables and porosity information at the nodal points are updated and the
 319 programme continues to the next time-step.

320

321 3. Verification

322 In this section, two examples of the model verifications are presented. The aim is to demonstrate the
 323 implementation accuracy and conceptual testing of the microbial processes in a coupled multiphase
 324 system.

325

326 3.1 Biofilm growth at a maximum rate

327 Considering $c_d^s \gg K'_s$ and $c_d^e \gg K'_e$ then $\frac{c_d^s}{K'_s + c_d^s} \cong 1$ and $\frac{c_d^e}{K'_e + c_d^e} \cong 1$, which lead to biofilm growth at a
 328 maximum rate (*i.e.* Equation (6b)). If biofilm growth is the only process of interest, Equation (4) yields,

$$\frac{\partial c_b^s}{\partial t} = k_+ c_b^s \quad (32)$$

329 Here k_+ represents the maximum growth rate and the growth is limited by neither the substrate nor the
 330 electron acceptor. The analytical solution of Equation (32) is: $c_b^s(t) = c_b^s(0)e^{k_+t}$.

331

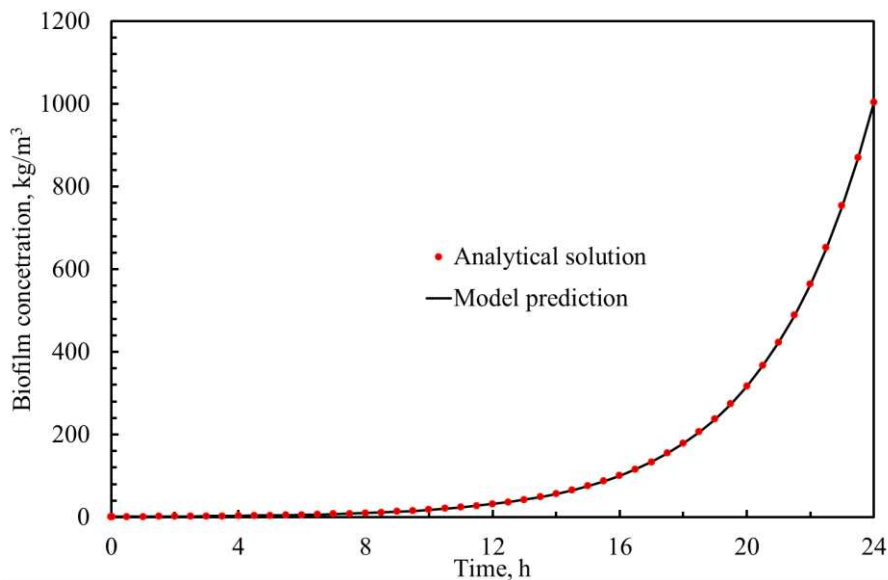


Figure 2 Comparison of the model predicted biofilm growth to the analytical solution.

332

333 For an initial biomass concentration, $c_b^s(0) = 1.0 \text{ kg/m}^3$ and $k_+ = 8.05 \times 10^{-5} \text{ s}^{-1}$, the results of biofilm
334 growth for 24 h are presented in Figure 2. The results show that the model predicted result is in good
335 agreement with the analytical solution.

336

337 *3.2 Biofilm growth in a multiphase system*

338 Growing biofilm in a multiphase system affects the flow of other phases. In this exercise, a 0.50 m by
339 0.05 m unsaturated sandstone sample is used to investigate such behaviour. It is assumed that no biocide
340 exists and the growth nutrient is constantly available to the microbes during the simulation. Therefore,
341 the substrate sink is omitted. It is also assumed that electron acceptors do not limit biofilm growth. The
342 sample domain is discretized into 100 equal-sized quadrilateral elements. The simulation is carried out
343 for 10 d.

344

345 *3.2.1 Simulation conditions*

346 Initial porewater pressure and poregas concentration are $-2 \times 10^3 \text{ Pa}$ and 4.036 mol/m^3 , respectively.
347 Initial biofilm concentration, $c_b^s = 0.001 \text{ kg/m}^3$ while the suspended biomass concentration, $c_b^l = 0$.
348 Concentration of the glucose substrate (c_d^s) during the simulation ($t \geq 0$) is $25 \times 10^{-3} \text{ kg/m}^3$.
349 At the left boundary, *i.e.* $x = 0$, gas is injected at the rate of $1.0 \times 10^{-4} \text{ mol/m}^2/\text{s}$. At the right boundary
350 *i.e.* $x = 0.50$, water pressure is fixed at $1.0 \times 10^6 \text{ Pa}$.

351

352 *3.2.2 Results*

353 The simulation parameters are presented in Table 1 and the results are in Figure 3. The results show
354 that the volumetric liquid content (θ_l) in the sample (at $x = 0.10$) increases rapidly from 0.21 to 0.249
355 by the supplied water from the fixed boundary. The flowing water displaces poregas and θ_g reduces.
356 The system remains nearly water saturated until the poregas pressure is high enough (after 11.52
357 minutes) to push the waterfront away from the gas injection face. Eventually the gas phase desaturates
358 the sample, resulting in the minimum or residual liquid saturation state ($s_r = 0.612$ which corresponds
359 to $\theta_l = 0.153$). The flow processes are relatively fast in sandstone due to weak water holding capacity.
360 It is noticeable from the results that the biofilm phase is relatively small during the first 24 h of the
361 simulation to exert any noticeable influence on the system. It grows rapidly after two days and reaches
362 a maximum after 5.8 d. Since the sample has already reached to the residual liquid saturation, biofilm
363 growth mainly occurred in the residual water volume. At this stage, the entire liquid volume disappears
364 into the biofilm phase and the remaining void volume is now occupied by the gas phase only. The active
365 porosity (n) is affected by the growing biofilm following the phase-volume relationships considered in
366 the model, *i.e.* Equations (1) and (2). After 5.8 d the sample porosity reaches to a minimum value of
367 0.149.

368

369 **Table 1** Parameter values for the verification of biofilm growth under multiphase flow condition.

Parameters	Values	Comments
<i>Medium and fluid flow parameters:</i>		
Porosity, n_0	0.25	
Intrinsic permeability, $K_{int,0}$	$3.98 \times 10^{-14} \text{ m}^2$	Mitchell et al. (2009)
Viscosity of water, μ_l	$0.9 \times 10^{-3} \text{ Pa s}$	Fredlund and Rahardjo (1993)
Viscosity of the gas, μ_g	$1.5 \times 10^{-5} \text{ Pa s}$	Mitchell et al. (2009)
Diffusion coefficient of the gas in air, D_g^0	$1.0 \times 10^{-5} \text{ m}^2/\text{s}$	Fredlund and Rahardjo (1993)
Henry's constant, H_c	$6.1 \times 10^{-4} \text{ mol/L/atm}$	Sander (2015); for nitrogen gas
Universal gas constant, R	8.3142 J/K/mol	
Absolute temperature, T	298 K	
<i>Biofilm Parameters:</i>		
Substrate utilisation rate, k_+	$8.01 \times 10^{-5} \text{ s}^{-1}$	Beyenal et al. (2003)
Yield coefficient, Y	0.628 kg/kg	Beyenal et al. (2003)
Monod half-saturation constant, K_S'	$26.9 \times 10^{-3} \text{ kg/m}^3$	Beyenal et al. (2003)
Endogenous death rate, k_-^e	$3.18 \times 10^{-7} \text{ s}^{-1}$	Taylor and Jaffe (1990)
Shear loss coefficient, b_s	$2.97 \times 10^{-6} \text{ s}^{-1}$	Rittmann (1982)
Biofilm density, ρ_b^s	65 kg/m^3	Peyton (1995)
<i>Water retention parameters:</i>		
α	0.79 m^{-1}	(van Genuchten, 1980)
β	10.4	(van Genuchten, 1980)
s_r	0.612	(van Genuchten, 1980)

370

371

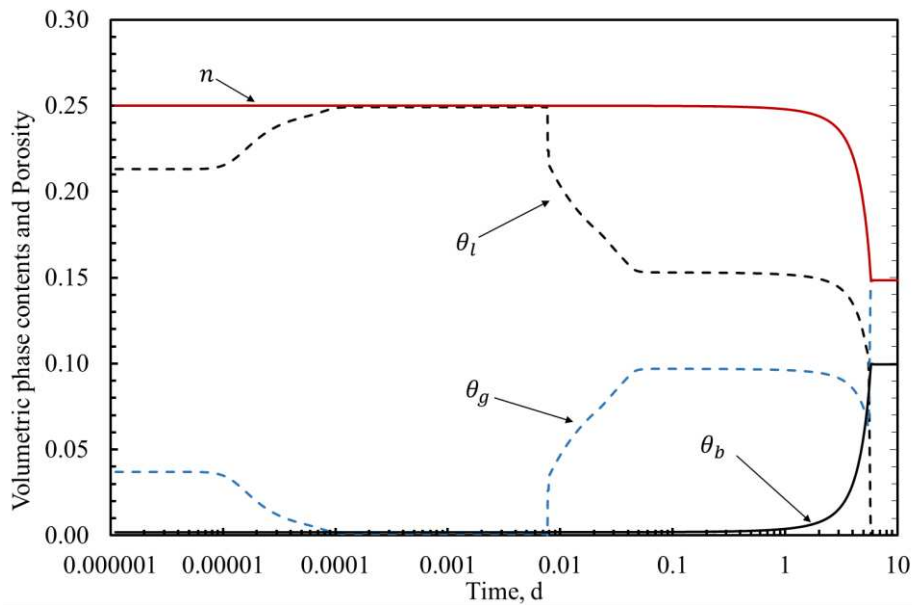


Figure 3 Biofilm growth in a two-phase flow system. Evolution of liquid phase, gas phase, biofilm phase and porosity. Please note, the vertical-axis scales both porosity and volumetric phase contents (θ). The black *dashed line* represents liquid content and the blue *dashed line* for gas content.

372

373 Figure 3 results show that, at any time, the corresponding volumetric contents of liquid, gas and biofilm
374 phases accumulate to the initial or unaffected system porosity (n_0). That suggests the coupled two-phase
375 processes are properly implemented in the model.

376

377 **4. Model Evaluation**

378 In this section, the model is evaluated against the experimental results of relevant interests. A
379 laboratory-based test has been chosen from the literature, which estimated the effects of biofilm growth
380 on physical properties of porous media.

381

382 *4.1 Model evaluation against experiments of Cunningham et al. (1991)*

383 Cunningham et al. (1991) carried out laboratory-scale experiments to investigate the effects of biofilm
384 growth on porosity and permeability of saturated porous media. 50 mm by 9 mm by 2 mm porous media
385 biofilm reactors were filled with either glass spheres, sand or a mixture of both glass and sand. The
386 experiments were performed under a constant piezometric boundary condition at the inlet and the outlet
387 and the volumetric flow rate was measured at a regular interval for 8 to 12 days. *Pseudomonas*
388 *aeruginosa* inoculum was used in their experiments. Since the bacteria form uniform biofilms, and the
389 kinetic and stoichiometric coefficients of this microorganism are well documented in literatures. Prior
390 to the tests, 5 mL of the concentrated inoculum was injected into each of the sterile reactors under
391 steady-state conditions to enable initial adsorption of the microbial cells and the formation of biofilms
392 in the solid phase. After 8 hours of settling period and significant sorption, reactors were flushed to
393 remove non-adsorbed cells and steady-state condition was established to begin the experiments. 25×10^{-3}
394 kg/m^3 glucose substrate was continuously supplied in the liquid phase of the porous media during the
395 tests.

396

397 *4.1.1 Simulation conditions*

398 Initial biofilm concentration in the reactor is calculated by measuring the bacterial cell weight in the 5
399 mL inoculum, which contained approximately 10^8 cells per mL of the inoculum (Cunningham et al.,
400 1991). Kim et al. (2012) reported that the dry weight of *Pseudomonas aeruginosa* cells varies between
401 6.4×10^{-11} to 2.8×10^{-12} g/cell. In this case, 1.0×10^{-12} g/cell is chosen to obtain the initial concentration of
402 biofilm, $c_b^s = 0.55 \text{ kg/m}^3$. Please note that due to lack of sufficient data, almost all of the cells in the
403 inoculum is assumed to be absorbed onto the solid phase. Concentration of suspended biomass in the
404 liquid phase is negligible; therefore, $c_b^l = 0$. Since, continuous supply of substrate was ensured during
405 the tests, its concentration during the simulation ($t \geq 0$) is $25 \times 10^{-3} \text{ kg/m}^3$. At $t = 0$, the saturated
406 porewater pressure $u_l = 100 \text{ Pa}$.

407 At the left ($x = 0$) and right ($x = 0.05$) boundaries, the applied hydrostatic pressures are 100 Pa and 350
408 Pa, respectively.

409
410
411
412
413
414
415
416
417
418
419

4.1.2 Parameters

Peyton (1995) reported volumetric mass density of a number of mono- and mixed-population biofilms. The values range between 5 and 130 kg/m³. For *Pseudomonas aeruginosa*, Peyton (1995) calculated the average biofilm density of 65.3 kg/m³. In this simulation, an average density of 85 kg/m³ is used. Parameters of substrate utilisation kinetics were collected from Beyenal et al. (2003) as, $k_+ = 8.01 \times 10^{-5} \text{ s}^{-1}$ and $K'_s = 26.9 \times 10^{-3} \text{ kg/m}^3$. The endogenous death rate, $k_e^e = 3.18 \times 10^{-7} \text{ s}^{-1}$ (Taylor and Jaffe, 1990). The shear detachment rate, $b_s = 3.21 \times 10^{-6} \text{ s}^{-1}$ (Rittmann, 1982). The porosity and original intrinsic permeabilities ($K_{int,0}$) of the 0.70 mm and 0.54 mm sand are 0.40 and 0.38 and $3.2 \times 10^{-10} \text{ m}^2$ and $2.2 \times 10^{-10} \text{ m}^2$, respectively. The viscosity of liquid water, $\mu_l = 0.895 \times 10^{-3} \text{ Pa s}$ (Fredlund and Rahardjo, 1993).

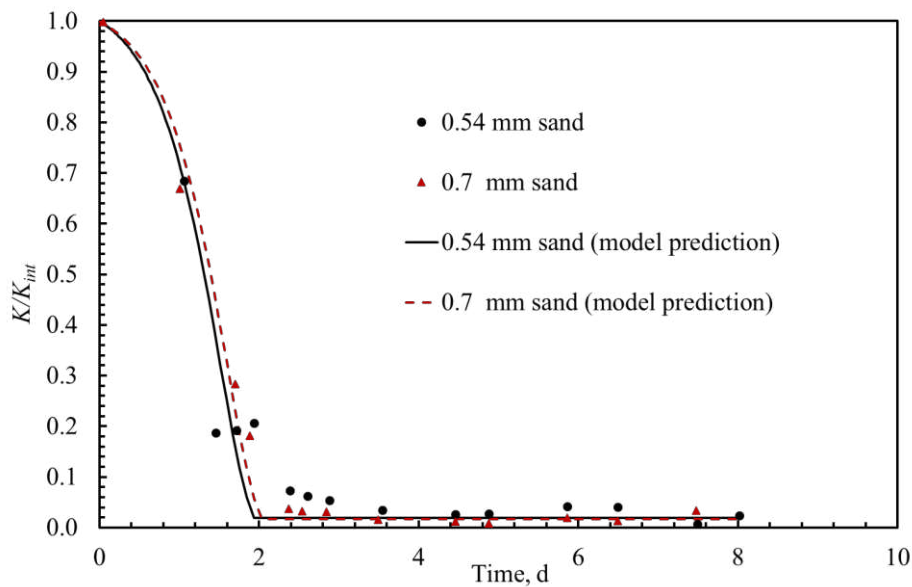


Figure 4 Permeability reduction due to biofilm growth in saturated biofilm reactors. Comparison between model results and the experimental results of Cunningham et al. (1991).

420

4.1.3 Results

422 The model domain is discretised into 100 equally sized quadrilateral elements. The simulation is carried
423 out for 8 d. Model predicted results for the 0.54 mm and 0.7 mm sand reactors are presented in Figure
424 4. The results are obtained at $x = 0.025 \text{ m}$. The simulation results are in good agreement with the results
425 of permeability reduction obtained by Cunningham et al. (1991). Biofilm growth affects the active
426 porosity of the sand reactors, which consequently alter the in-situ intrinsic permeability of the media
427 following Equation (22). Permeability of both reactors drops to the minimum relatively fast (in around
428 2 days) and remains steady until the end of the simulation. The fast growing biofilm undermines the
429 overall impacts of biomass reductions (endogenous death and shear loss in this case). The minimum

430 permeability predicted in these simulations are approximately 2% of the original value, which is within
431 the range of values (between 1 and 5%) observed by Cunningham et al. (1991).

432

433 5. Application

434 In this section, the model has been applied to investigate subsurface microbial process. Four sets of
435 simulations are presented to observe i) microbial growth at various gas injection rates, ii) effect of pH
436 on the growth, iii) microbial respiration in a fully coupled multiphase condition and, iv) microbial
437 fermentation and gas production. The model domain is a 0.5 m by 0.125 m sandstone core. The domain
438 is discretized into 100 quadrilateral elements with finer spatial discretization at the boundaries, as shown
439 in Figure 5.

440

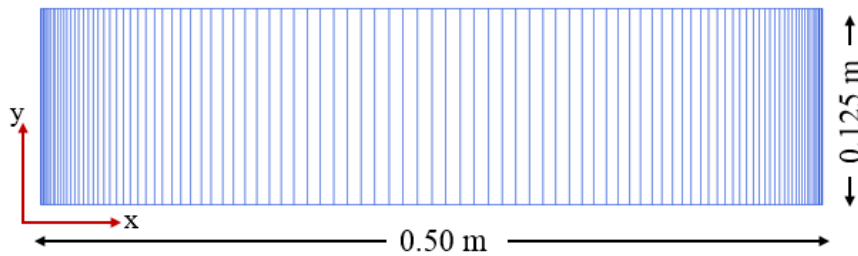


Figure 5 Simulation mesh of the sample domain.

441

442 5.1 Biofilm growth in two-phase condition

443 In these simulations, biofilm growth is investigated under simultaneous flow of water and a gas. The
444 objective is to investigate the response of microbial growth and its effect on porous media flow
445 properties at different gas injection rates. Two tests have been carried out, where injection rate in Test
446 I is higher than in Test II. It has been assumed that the substrate is abundantly available to microbes and
447 the growth is not limited by an electron acceptor. The simulations have been carried out for 24 h.

448

449 5.1.1 Initial and boundary conditions

450 Initial porewater pressure (u_l) in the core is -2×10^3 Pa, gas concentration, $c_g = 4.04$ mol/m³, biofilm
451 concentration, $c_b^s = 1.0$ kg/m³ and the concentration of suspended biomass, $c_b^l = 0$.

452 At the right boundary, *i.e.* at $x = 0.50$ gas is injected at the rate of 1.0×10^{-6} mol/m²/s and 1.0×10^{-7}
453 mol/m²/s in Test I and Test II, respectively. The left side of the core (*i.e.* at $x = 0$) is fixed at a water
454 pressure of 100 Pa. The left boundary and the right boundary are impermeable for gas and water,
455 respectively. Concentration of the glucose substrate during the simulation ($t \geq 0$) is 25×10^{-3} kg/m³.

456

457 5.1.2 Parameters

458 The simulation parameters are listed in Table 2.

459

460 **Table 2** Parameter values for Test I and Test II simulations.

Parameters	Values	Comments
<i>Medium and fluid flow parameters:</i>		From Table 1
<i>Biofilm Parameters:</i>		
Substrate utilisation rate, k_+	$8.01 \times 10^{-5} \text{ s}^{-1}$	Beyenal et al. (2003)
Monod half-saturation constant, K'_S	$26.9 \times 10^{-3} \text{ kg/m}^3$	Beyenal et al. (2003)
Endogenous death rate, k_-^e	$3.18 \times 10^{-7} \text{ s}^{-1}$	Taylor and Jaffe (1990)
Shear loss coefficient, b_s	$2.97 \times 10^{-6} \text{ s}^{-1}$	Rittmann (1982)
Biofilm density, ρ_b^s	65 kg/m^3	Peyton (1995)
<i>Water retention parameters:</i>		From Table 1

461

462 5.1.3 Results

463 The simulation results are obtained from the gas injection boundary *i.e.* $x = 0.5$. The results in Figure 6
 464 show that the liquid saturation in the core increases rapidly from 0.85 to 0.87 due to the fixed hydrostatic
 465 boundary. The core remains nearly water saturated until the poregas pressures is large enough to drive
 466 the waterfront away from the gas injection face. As expected, the core starts to desaturate earlier in Test
 467 I than in Test II. The core reaches to the minimum liquid saturation after 4.2 h in Test I but in Test II
 468 the liquid saturation reduces to 0.68 after 24 h of simulation. Figure 7 shows the results of biofilm
 469 growth and its effects on the core porosity. During the saturation and desaturation period, biofilm phase
 470 remains too small to exert any noticeable change on the porosity of the core. The impact escalates with
 471 the net growth of the biofilm phase which is limited by the volume of available water in the core.
 472 Biofilm concentration and porosity reduction in Test II is larger than in Test I, since the desaturation of
 473 the core in Test II is slower which provides more time for the biofilm to grow before liquid phase
 474 reaches to the minimum. The results show that the core porosity is reduced to 0.16 and 0.15 in Test I
 475 and II which are 64% and 60% of the original unaffected porosity, respectively. Figure 8 shows the
 476 evolution of gas pressure (and concentration) for the corresponding gas injection rates. After 24 h the
 477 observed gas pressure in Test I is 188.8 kPa while in Test II 14.8 kPa.

478

479 At the early stages of the simulations, when fluid flow processes are dominant, biofilm phase remains
 480 considerably small and liquid shear loss is negligible. At the later stages, when biofilm growth is
 481 significant, fluid flow is minimum and shear loss is insignificant. For the current parameter values, the
 482 results suggest that under constant supply of substrates, growth processes surpass the overall decay rates
 483 and promote net accumulation of biofilm in the sandstone core. However it is worthwhile to mention
 484 that the water phase in natural soils at residual saturation might be discontinuous and the notion of
 485 uninterrupted supply of growth nutrients to the microbes in such condition may lead to an
 486 overestimation.

487

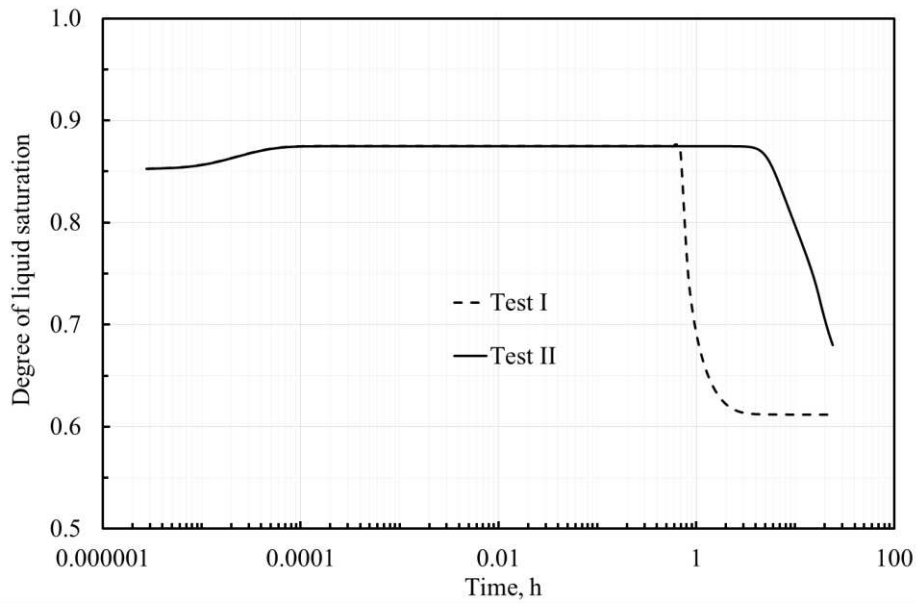


Figure 6 Evolution of water saturation in the sandstone core under simultaneous flow of water and gas. Gas injection rates for Test I and Test II simulations are 1.0×10^{-6} mol/m²/s and 1.0×10^{-7} mol/m²/s, respectively.

488

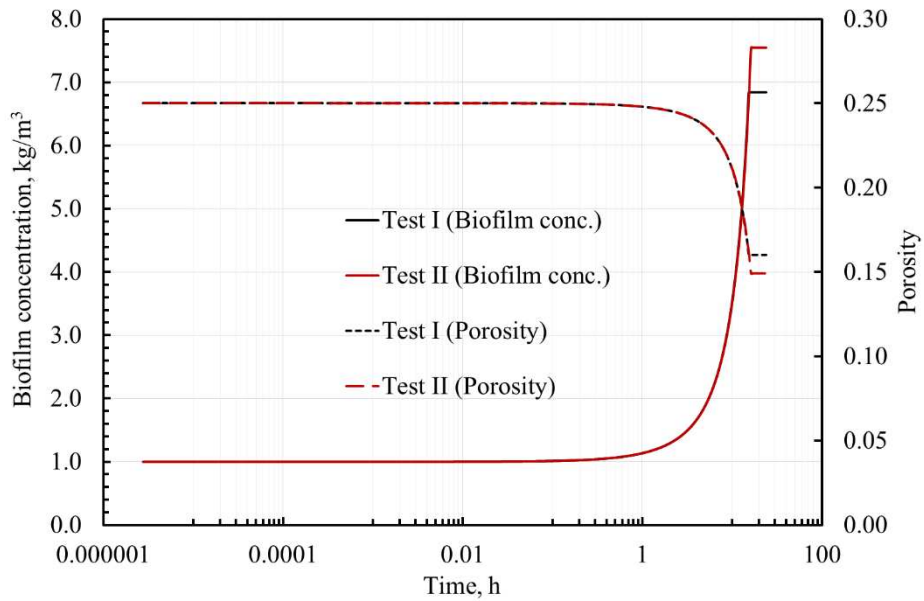


Figure 7 Biofilm concentration and the effect on sandstone porosity for Test I and II. The *solid lines* represent biofilm concentration on the left vertical axis and the *dashed lines* represent porosity on the right vertical axis.

489

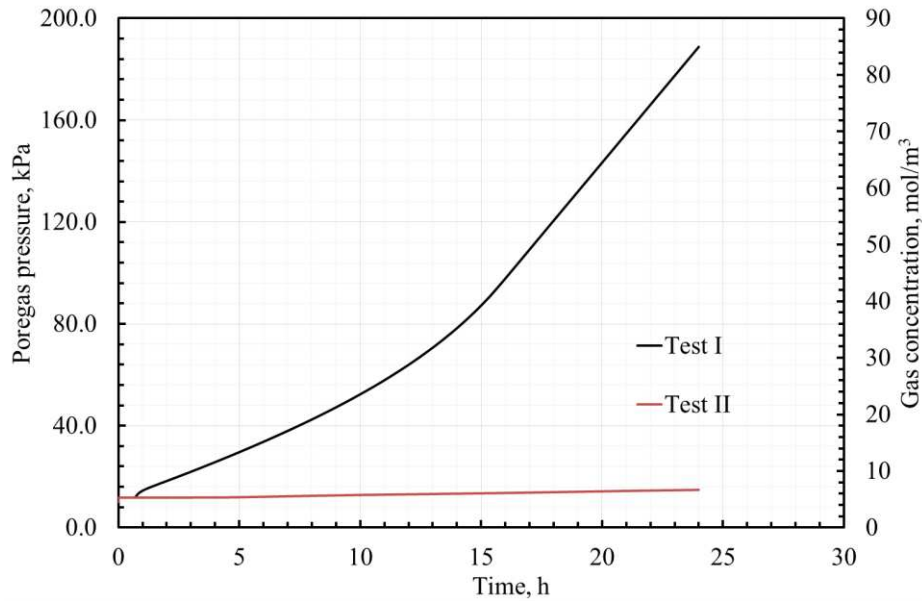


Figure 8. Gas pressure (concentration) evolution during Test I and II simulations.

490

491 5.2 Effect of pH on biofilm growth

492 The aim of this section is to observe biofilm growth under variable pH. Two set of simulations have
 493 been carried out in that regard. In the first set biofilm growth is predicted under a constant pH. In the
 494 second simulation injection and dissolution of CO₂ gas in the sandstone water has been considered.
 495 Aqueous carbon dioxide, CO₂ (aq), reacts with water and forms aqueous carbonic acid, H₂CO₃. The
 496 carbonic acid may lose up to two protons to form bicarbonate and carbonate species. The released proton
 497 eventually reduces the pH of the system. The overall reaction:



498 The reactions (R1) have been modelled using PHREEQC. To emphasis on the effect of pH on biofilm
 499 growth following assumptions have been made at this stage: substrate concentration remains constant
 500 throughout the simulation, growth is not limited by electron acceptors, substrate doesn't influence the
 501 solution pH and microbial metabolism of this substrate doesn't produce any gas. The simulations have
 502 been carried out for 10 h.

503

504 5.2.1 Initial and boundary condition

505 In both simulations, initially fully water saturated sandstone core is assumed to contain 1.0 kg/m³ of
 506 biofilm at pH 7.0. Concentration of the substrate during the simulation ($t \geq 0$) is 25×10^{-3} kg/m³.

507 In simulation 1 (constant pH), fixed hydrostatic pressure of 100 Pa is considered at the left and right
 508 boundaries. In simulation 2 (variable pH), fixed hydrostatic pressure of 100 Pa is applied at the left
 509 boundary *i.e.* at $x = 0$ and a constant CO₂ gas injection rate of 1.0×10^{-9} mol/m²/s is applied at the right

510 boundary ($x = 0.50$). The left boundary for the gas and right boundary for water are assumed
 511 impermeable in simulation 2.

512

513 *5.2.2 Parameters*

514 The parameters are listed in Table 3. PHREEQC database “*Phreeqc.dat*” (wwwbrr.cr.usgs.gov, 2017)
 515 is used in Simulation 2. Reaction parameters which are required for the simulation *i.e.* thermodynamic
 516 equilibrium constant (\log_k) and reaction enthalpy (Δ_h) are available in the database. An example
 517 of PHREEQC input data file for simulation 2 is presented in Table 4. Please note that the gas dissolution
 518 (R1.1) is calculated using PHREEQC and therefore, Henry’s constant has not been mentioned
 519 explicitly.

520

521 **Table 3** Parameter values for simulation 1 (constant pH) and 2 (variable pH).

Parameters	Simulation 1	Simulation 2	Comments
<i>Medium and fluid flow parameters:</i>			
Porosity, n_0		0.25	
Intrinsic permeability, $K_{int,0}$		$3.98 \times 10^{-14} \text{ m}^2$	Mitchell et al. (2009)
Viscosity of water, μ_l		$0.9 \times 10^{-3} \text{ Pa s}$	Fredlund and Rahardjo (1993)
Viscosity of the gas, μ_g	-	$1.5 \times 10^{-5} \text{ Pa s}$	Mitchell et al. (2009)
Gas diffusion coefficient, D_g^0	-	$1.0 \times 10^{-5} \text{ m}^2/\text{s}$	Fredlund and Rahardjo (1993)
Universal gas constant, R	-	8.3142 J/mol	
Absolute temperature, T	-	298 K	
<i>Biofilm Parameters:</i>			
Substrate utilisation rate, k_+		$8.01 \times 10^{-5} \text{ s}^{-1}$	Beyenal et al. (2003)
Yield coefficient, Y		0.628 kg/kg	Beyenal et al. (2003)
Half-saturation constant, K'_s		$26.9 \times 10^{-3} \text{ kg/m}^3$	Beyenal et al. (2003)
Endogenous death rate, k_-^e		$3.18 \times 10^{-7} \text{ s}^{-1}$	Taylor and Jaffe (1990)
Shear loss coefficient, b_s	-	$2.97 \times 10^{-6} \text{ s}^{-1}$	Rittmann (1982)
Biocide decay constant, c_-^b	-	$8.7 \times 10^{-4} \text{ s}^{-1}$	Ebigbo et al. (2010)
Biocide decay constant, c_c	-	3	Ebigbo et al. (2010)
Biofilm density, ρ_b^s		65 kg/m^3	Peyton (1995)
<i>Parameters for pH dependent growth:</i>			
Growth constant, k_0^p	-	$5.19 \times 10^{-5} \text{ s}^{-1}$	(Tan et al., 1998)
Ionisation constant, K_1^p	-	$9.15 \times 10^{-7} \text{ mol/L}$	(Tan et al., 1998)
<i>Water retention parameters:</i>			
	-	From Table 1	

522

523

524 **Table 4** An example of PHREEQC input data file for the simulation 2.

```

TITLE Dissolution of CO2 gas in water and pH change

SOLUTION_SPECIES
CO3-2 + 2 H+ = CO2 + H2O
  log_k      16.681
  delta_h    -5.738 kcal

PHASES
CO2(g)
  CO2 = CO2          # dissolution of CO2 in water
  log_k      -1.468  # Gas : Liquid partitioning following Henry's law
  delta_h    -4.776 kcal # reaction enthalpy

SOLUTION 1 Pure water          # solution definition/ composition
  -units mol/kgw
  pH      **                  # data provided from the transport module
  C       **                  # total carbon; data provided from the transport module

GAS_PHASE 1
  -fixed_volume
  CO2(g)   **                  # data provided from the transport module

End

```

525

526 *5.2.3 Results*

527 Development of the biofilm and change in porosity with time at the right boundary ($x = 0.5$) are
528 presented in Figure 9. The simulation results show significant biofilm growth at constant pH of 7.0
529 (Simulation 1). In contrast limited biofilm growth is observed at this location under CO₂ injection
530 (Simulation 2). The lack of growth in simulation 2 is associated with the reduction of pH. According to
531 Equation (12), at lower pH, ionisation state of the system becomes less suitable for the microbe to bind
532 substrates and therefore, the growth is hindered. Figure 10 shows that injected CO₂ reduces pH from
533 initial 7.0 to 5.5 in a short span of time which retards the pH-dependent growth rate from 4.68×10^{-5} to
534 $6.92 \times 10^{-6} \text{ s}^{-1}$ (inset diagram), although the substrate is abundantly available. Increasing CO₂ pressure
535 also accelerates biocide-induced death. Since CO₂ gas is highly soluble in water, the gas phase pressure
536 build up is limited and as a result, the liquid saturation at this location remains relatively high (Figure
537 11). The modelling capacity of the linked COMPASS-PHREEQC platform has been demonstrated via
538 simulation 2.

539

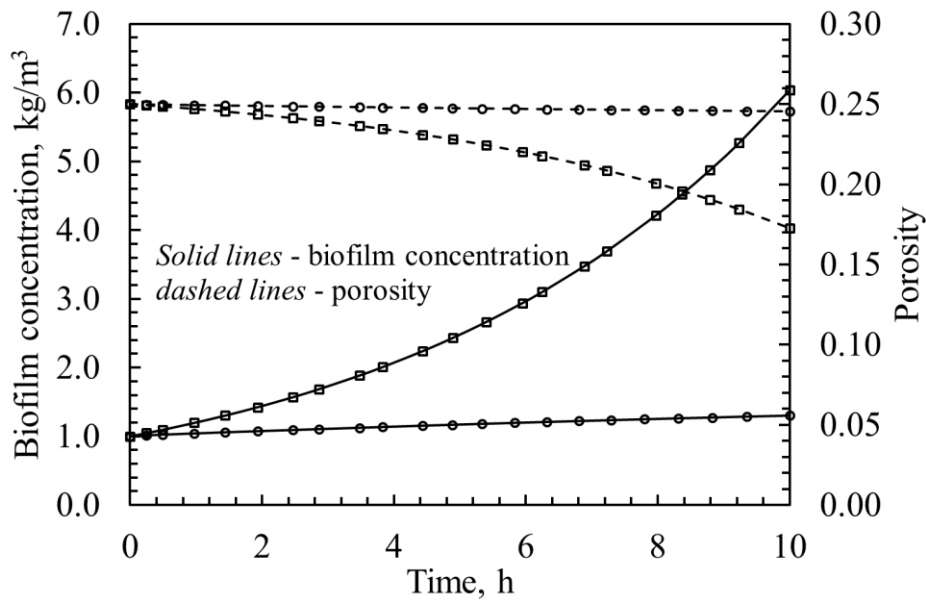


Figure 9 Biofilm growth and porosity evolution at the gas injection boundary, $x = 0.50$. The symbol (\square) represents simulation 1 *i.e.* constant pH and (\circ) for Simulation 2 *i.e.* variable pH. The *solid lines* represents biofilm concentration on the left vertical axis and the *dashed lines* represents porosity on the right vertical axis.

540

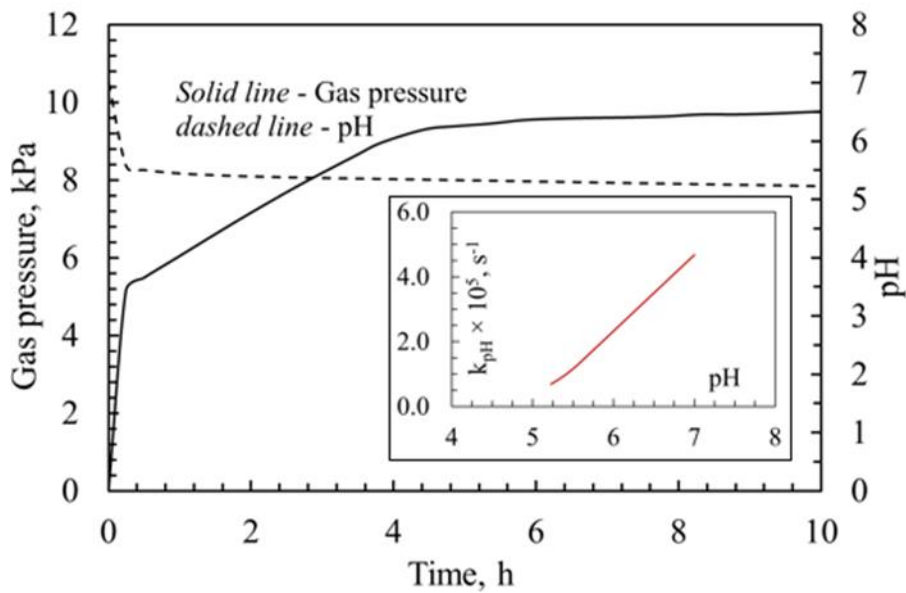


Figure 10 Evolution of CO₂ pressure and pH at the gas injection boundary in Simulation 2. The *dashed line* represents pH on the right vertical axis and the *solid line* for gas pressure on the left vertical axis. The diagram inset shows the effect of pH on the growth rate, k_{pH} , during the simulation.

541

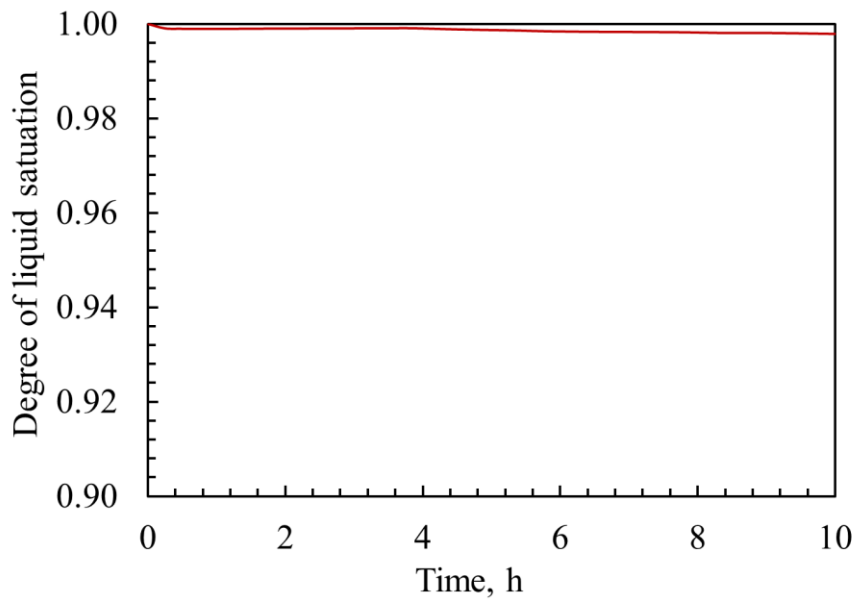


Figure 11 Change in liquid saturation with time at the gas injection boundary during simulation 2.

Please note the scale of vertical axis ranges between 0.9 and 1.0.

542

543 *5.3 Microbial respiration in coupled two-phase flow condition*

544 In this simulation, the model has been applied to investigate microbial respiration under a two-phase
 545 flow condition. During respiration microbes harness the energy released from a reduced species in the
 546 environment to an oxidized species (Bethke, 2008). Therefore the growth is limited by both substrate
 547 and an electron acceptor. It has been assumed that the microbial species does not produce any gas during
 548 respiration. The simulation has been carried out for 24h.

549

550 *5.3.1 Initial and boundary conditions*

551 Initial conditions for this simulation are: porewater pressure -2.0×10^3 Pa, substrate concentration (c_d^s)
 552 1.0 kg/m^3 , dissolved oxygen concentration (c_d^e) 1.0 kg/m^3 , gas concentration 1.0 mol/m^3 , biofilm
 553 concentration, 0.1 kg/m^3 and the concentration of suspended biomass, $c_b^l = 0$.

554 At the boundary, $x = 0$, concentrations of substrate and dissolved oxygen are fixed at 3.0 and 1.0 kg/m^3 ,
 555 respectively. At the right boundary, $x = 0.50$, gas is injected at the rate of $3.0 \times 10^{-6} \text{ mol/m}^2/\text{s}$ and the left
 556 boundary is considered impermeable for the gas. Fixed hydrostatic pressures of 1.0×10^3 and 2.0×10^2 Pa
 557 are maintained at the left and right boundary, respectively.

558

559 *5.3.2 Parameters*

560 The simulation parameters are listed in Table 5.

561

562 **Table 5** Parameter values for the simulation of microbial respiration in a two-phase flow

Parameters	Values	Comments
<i>Medium and fluid flow parameters:</i>		
Porosity, n_0	0.25	
Intrinsic permeability, $K_{int,0}$	$3.98 \times 10^{-14} \text{ m}^2$	Mitchell et al. (2009)
Viscosity of water, μ_l	$0.9 \times 10^{-3} \text{ Pa s}$	Fredlund and Rahardjo (1993)
Viscosity of the gas, μ_g	$1.5 \times 10^{-5} \text{ Pa s}$	Mitchell et al. (2009)
Henry's constant	$6.1 \times 10^{-4} \text{ mol/L/atm}$	Sander (2015); for nitrogen gas
Gas diffusion coefficient, D_g^0	$1.0 \times 10^{-5} \text{ m}^2\text{s}^{-1}$	Fredlund and Rahardjo (1993)
Diffusion coefficient of glucose in water, $D_d^{s,0}$	$6.70 \times 10^{-10} \text{ m}^2\text{s}^{-1}$	Cussler (1997)
Diffusion coefficient of dissolved oxygen in water, $D_d^{e,0}$	$2.10 \times 10^{-9} \text{ m}^2\text{s}^{-1}$	Cussler (1997)
Longitudinal dispersion coefficient, α_L	1.0 m	Gelhar et al. (1992)
Universal gas constant, R	8.3142 J/K/mol	
Absolute temperature, T	298 K	
<i>Biofilm Parameters:</i>		
Substrate utilisation rate, k_+	$8.05 \times 10^{-5} \text{ s}^{-1}$	Beyenal et al. (2003)
Substrate yield coefficient, Y	0.628 kg/kg	Beyenal et al. (2003)
Substrate half-saturation constant, K'_s	$26.9 \times 10^{-3} \text{ kg/m}^3$	Beyenal et al. (2003)
Oxygen yield coefficient, F	0.635 kg/kg	Beyenal et al. (2003)
Oxygen half-saturation constant, K'_e	$1.18 \times 10^{-3} \text{ kg/m}^3$	Beyenal et al. (2003)
Endogenous death rate, k_-^e	$3.18 \times 10^{-7} \text{ s}^{-1}$	Taylor and Jaffe (1990)
Shear loss coefficient, b_s	$2.97 \times 10^{-6} \text{ s}^{-1}$	Rittmann (1982)
Biofilm density, ρ_b^s	65 kg/m^3	Peyton (1995)
<i>Water retention parameters:</i>	From Table 1	

563

564 **5.3.3 Results**

565 Evolution results of the components have been collected from three locations *i.e.* $x = 0, 0.15$ and 0.45
566 m of the sample (Figure 5). Figure 12a presents biofilm growth and its effects on the medium porosity.
567 The results show maximum growth at the nutrient source and away from the source it is affected by the
568 supply of nutrients as well as liquid saturation, which is influenced by the injected gas. Loss of porosity
569 continues at variable rates with biofilm growth along the sample (*i.e.* at 0.15m , porosity reduces 5.2%
570 to 0.237) but reaches the minimum, at the nutrient source, after 19h approximately. Biofilm
571 concentration and porosity profiles after 24 h are presented in Figure 13a. The results indicate that the
572 biofilm growth and porosity loss are negligible closer to the gas injection boundary. Although, at the
573 early stages of the simulation biofilm grows by utilising the available substrate and oxygen, the growth
574 is very small and un-detectable at the scale used in the y-axis. The growth period is short near this
575 boundary, since the sample de-saturates rapidly by the injected gas and it retards the flow of substrate
576 and oxygen to the microbes.

577

578 Figure 12b shows the evolution of substrate and dissolved oxygen concentrations in the sample. Initial
579 concentrations of both substrate and dissolved oxygen were 1.0 kg/m^3 . However, at the boundary,

580 substrate concentration instantly reaches to the applied concentration of 3.0 kg/m^3 . Along the sample
581 domain, the convective-dispersive transport of substrate and dissolved oxygen are affected by biofilm
582 growth, porosity and permeability reduction as well as gas pressure evolution. The results show that, at
583 0.15 m from the source, substrate concentration reaches to a maximum of 1.17 kg/m^3 after 1 h and
584 reduces to zero after 9 h . Meanwhile, the dissolved oxygen concentration reduces from 1.0 kg/m^3 to
585 0.18 kg/m^3 after 9 h and remains steady for the rest of the simulation. From the result of biofilm growth
586 at this location, Figure 12a, it can be noticed that after 9 h the growth suspends due to lack of substrate,
587 which consequently ceases the consumption of dissolved oxygen. Concentration profiles of the nutrients
588 (substrate and electron acceptor) are presented in Figure 13b after 5 h and 9 h of simulation. Since, the
589 elevated gas pressure de-saturates the sample, both substrate and dissolved oxygen concentrations are
590 negligible within the vicinity (note the concentration evolution of nutrients at 0.45 m in Figure 12b) of
591 the gas injection boundary. The ‘hump shape’ near the end of the concentration profiles (Figure 13b)
592 occurs due to simultaneous flow of nutrients driven by hydraulic gradient from one side and gas-
593 pressure driven water flow from the other side. No hump is visible for the substrate after 9 h , since all
594 of it has been used in the microbial respiration.

595

596 Evolution of gas concentration and liquid saturation is presented in Figure 12c. Since, no outflow of
597 gas has been allowed, its concentration across the sandstone sample increases rapidly from initial 1.0
598 mol/m^3 to 2.1 mol/m^3 at the onset of the simulation due to reduction of gas phase volume. The fixed
599 hydrostatic pressures at the boundaries almost saturates ($>99\%$) the sample. However the constant
600 injection of gas increases the concentration close to the boundary and pushes the waterfront away. After
601 approximately 3 h gas pressure at 0.05 m from the injection boundary increases sharply and decreases
602 the liquid saturation (to 0.67 after 5 h). Therefore biofilm growth at this location (Figure 12a), as
603 mentioned earlier, is negligible. The gas concentration and liquid saturation profiles are presented in
604 Figure 13c. The results are plotted after 19 h simulation period when the porosity of the left boundary
605 reduces to zero *i.e.* the face becomes impermeable due to bio-clogging.

606

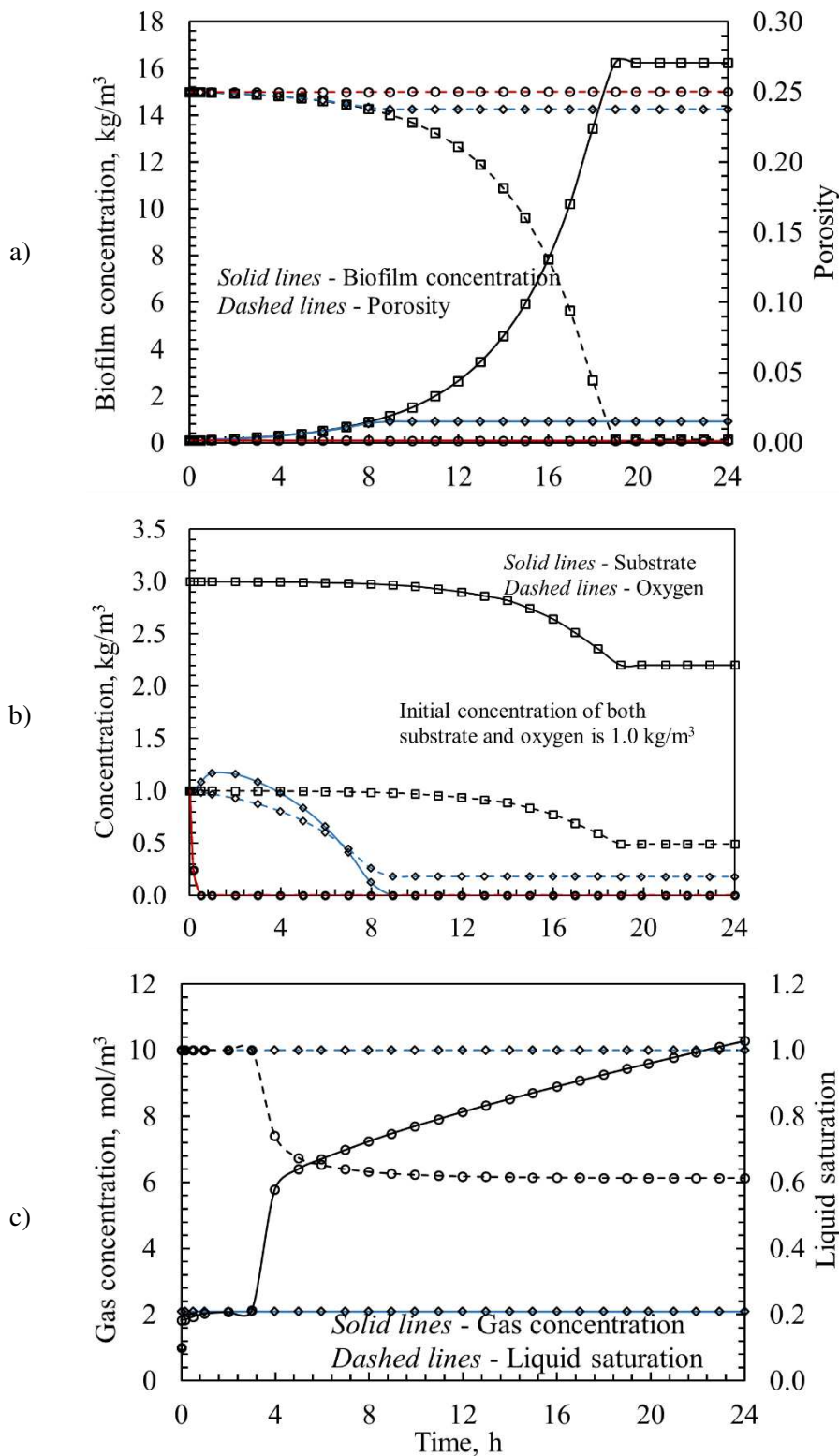


Figure 12 Evolution of a) biofilm and porosity, b) substrate and electron acceptor, c) gas concentration and liquid saturation in the sandstone sample. The symbols (\square), (\diamond), (\circ) represent the results at $x = 0, 0.15$ and 0.45m , respectively. Please note that in c) only the results at 0.15 and 0.45m are presented.

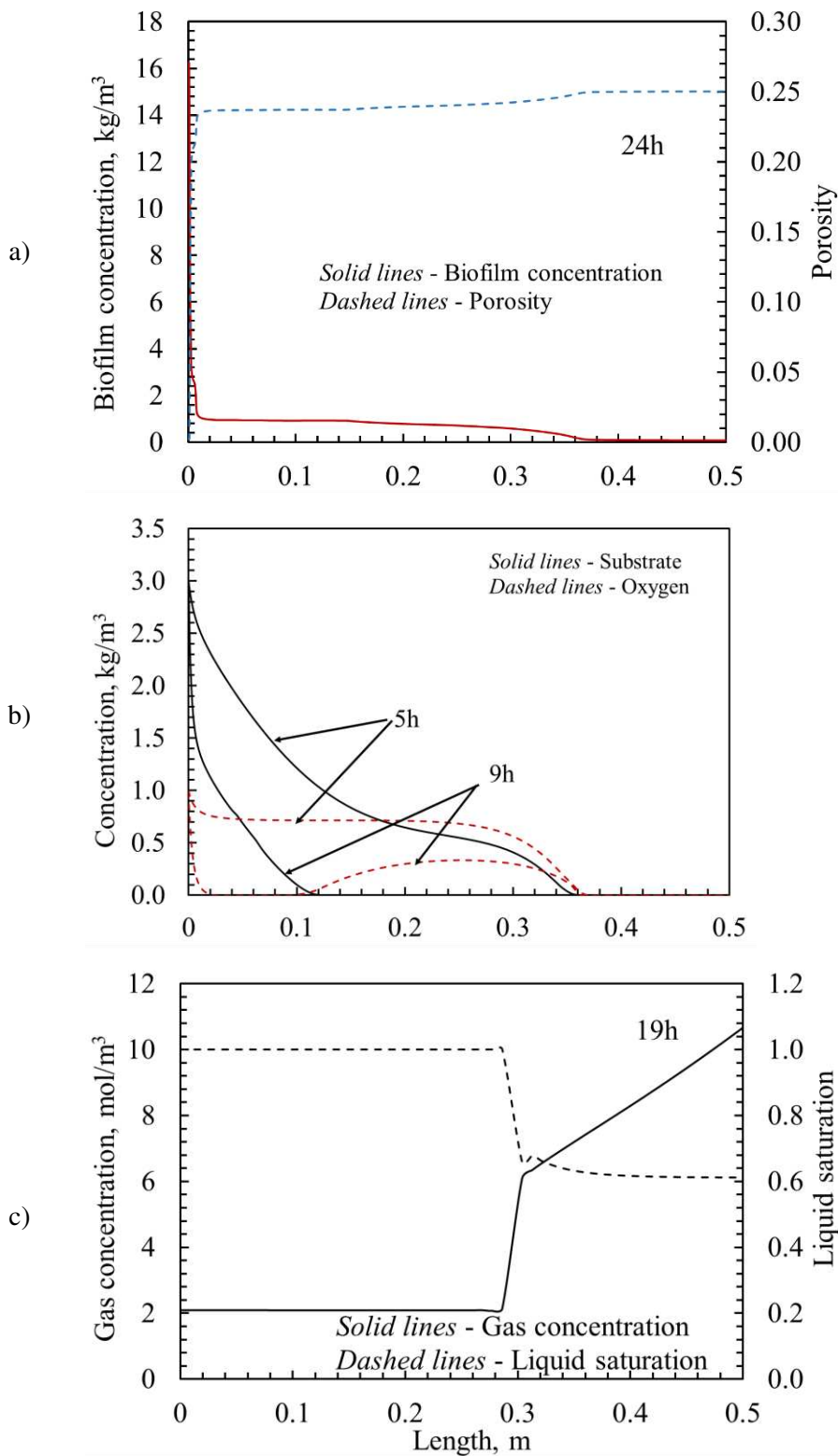


Figure 13 Profiles of a) biofilm and porosity, b) substrate and electron acceptor, c) gas concentration and liquid saturation along the length of the sandstone sample during microbial respiration under coupled flow.

610 *5.4 Microbial growth via fermentation and production of CO2 gas*

611 In this section, the model has been applied to predict microbial fermentation which occurs when
612 microbes metabolise substrates in absence of suitable electron acceptors in the medium. Microbial
613 fermentation of glucose substrate and the production of ethanol and CO2 gas as reaction by product is
614 considered. The overall chemical reaction:



615 The production of CO2 in the model is obtained from the reaction stoichiometry *i.e.* for one mole of
616 glucose metabolised two moles of CO2 gas is produced. The reaction has been modelled within the
617 COMPASS model. Therefore the geochemical model has not been used in this simulation. Since pH is
618 buffered in water-ethanol mixture and its changes are smaller, the effect of pH on microbial processes
619 has been ignored. The simulation has been carried out for 10 h.

620

621 *5.4.1 Initial and boundary conditions*

622 Initially the saturated sandstone sample contained 1.0 kg/m³ of glucose substrate and 0.1 kg/m³ of
623 biofilm and no gas.

624 At the left boundary, $x = 0$, substrate concentration is fixed at 3.0 kg/m³. Fixed hydrostatic pressures of
625 1.0×10^3 and 2.0×10^2 Pa has been applied the left and right boundary, respectively. Boundaries are
626 considered impermeable, *i.e.* no-flow condition, for the gas.

627

628 *5.4.2 Parameters*

629 The parameters for the simulation are presented in Table 6. Henry's constant for CO2 in water at 298K
630 is 1600 atm or 3.4×10^{-2} mol/L/atm (Sander, 2015). However in water-ethanol mixture, at low ethanol
631 concentration (less than 0.1 mole fraction), Henry's constant is 2240 atm (Postigo and Katz, 1987),
632 which makes CO2 less soluble.

633

634 *5.4.3 Results*

635 The results of this simulation are presented in Figure 14 (evolution of variables at $x = 0$ and 0.45m) and
636 Figure 15 (profiles of variables). The results in Figure 14a and 15a show that biofilm concentration
637 varies from 1.44 kg/m³ to 1.33 kg/m³ and porosity from 0.229 to 0.231 between the two boundaries.
638 Biofilm concentration near the source of substrate is slightly higher than the opposite boundary (Figure
639 14a), which are due to the supply and availability of glucose substrate in the sample (Figure 14b). The
640 supply of substrate also influences the concentration of CO2(g) and saturation level (Figure 14c and
641 Figure 15c). Within the vicinity of the source, elevated microbial metabolism results into little more
642 production of CO2(g) than the other end. The gas pressure continues to build up following the
643 fermentation reaction and de-saturation of the sample continues. The observed saturations (Figure 14c)
644 after 10 h at $x = 0$ and 0.50 m are 81.4% and 87.9%, respectively.

645

646 **Table 6** Simulation parameters for predicting microbial fermentation

Parameters	Values	Comments
<i>Medium and fluid flow parameters:</i>		
Porosity, n_0	0.25	
Intrinsic permeability, $K_{int,0}$	$3.98 \times 10^{-14} \text{ m}^2$	Mitchell et al. (2009)
Viscosity of water, μ_l	$0.9 \times 10^{-3} \text{ Pa s}$	Fredlund and Rahardjo (1993)
Viscosity of the gas, μ_g	$1.5 \times 10^{-5} \text{ Pa s}$	Mitchell et al. (2009)
Diffusion coefficient of the gas in air,	$1.0 \times 10^{-5} \text{ m}^2/\text{s}$	Fredlund and Rahardjo (1993)
Henry's constant, H_c	$2.04 \times 10^{-2} \text{ mol/L/atm}$	Calculated
Universal gas constant, R	8.3142 J/K/mol	
Absolute temperature, T	298 K	
<i>Biofilm Parameters:</i>		
Substrate utilisation rate, k_+	$8.01 \times 10^{-5} \text{ s}^{-1}$	Beyenal et al. (2003)
Yield coefficient, Y	0.628 kg/kg	Beyenal et al. (2003)
Monod half-saturation constant, K'_S	$26.9 \times 10^{-3} \text{ kg/m}^3$	Beyenal et al. (2003)
Endogenous death rate, k_-^e	$3.18 \times 10^{-7} \text{ s}^{-1}$	Taylor and Jaffe (1990)
Shear loss coefficient, b_s	$2.97 \times 10^{-6} \text{ s}^{-1}$	Rittmann (1982)
Biofilm density, ρ_b^s	65 kg/m ³	Peyton (1995)
<i>Water retention parameters:</i>	From Table 1	

647

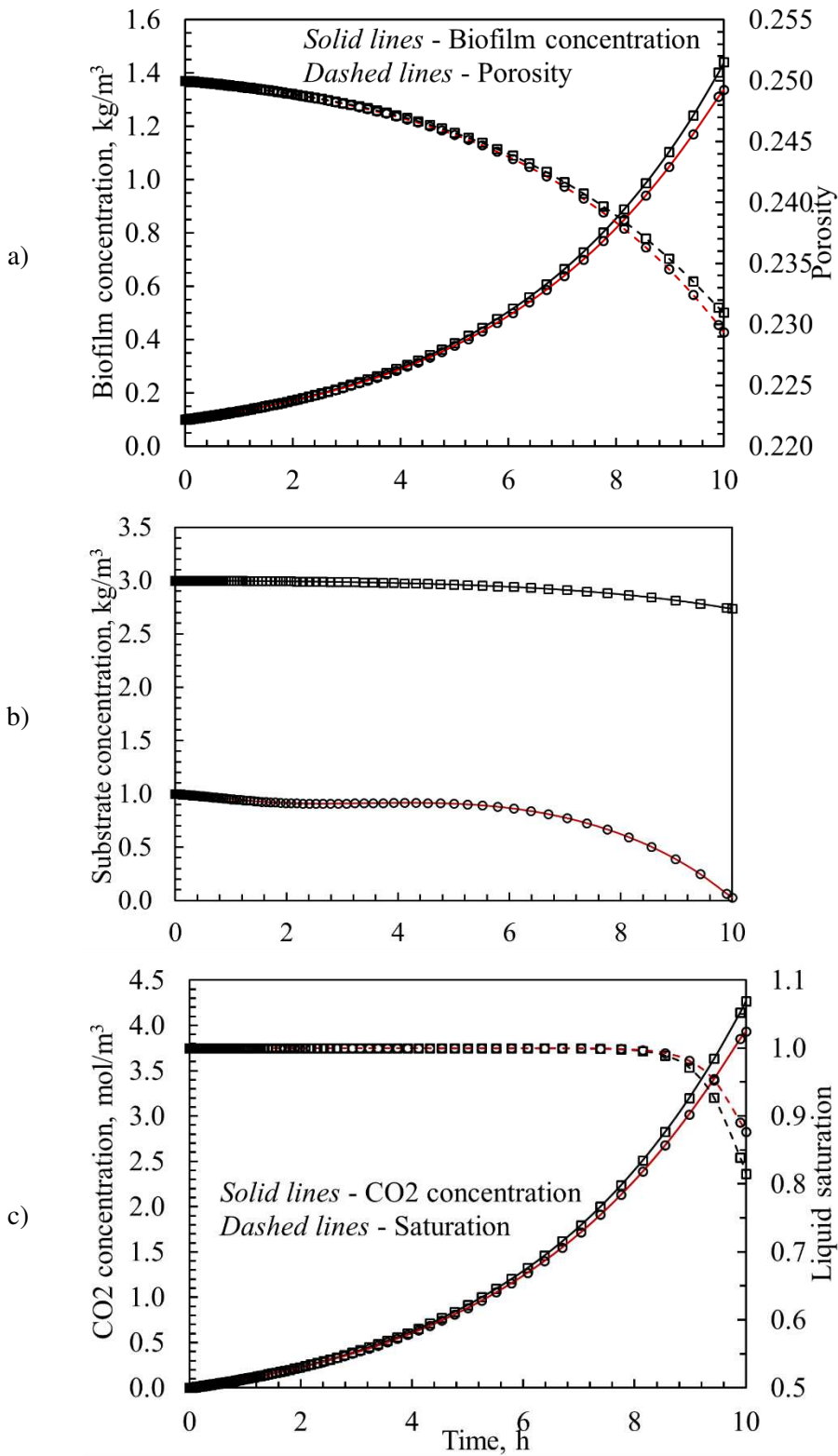


Figure 14 Evolution of a) biofilm and porosity, b) substrate, c) gas concentration and liquid saturation in the sandstone sample. The symbols (\square) and (\circ) represent the results at $x = 0$ and 0.45m , respectively.

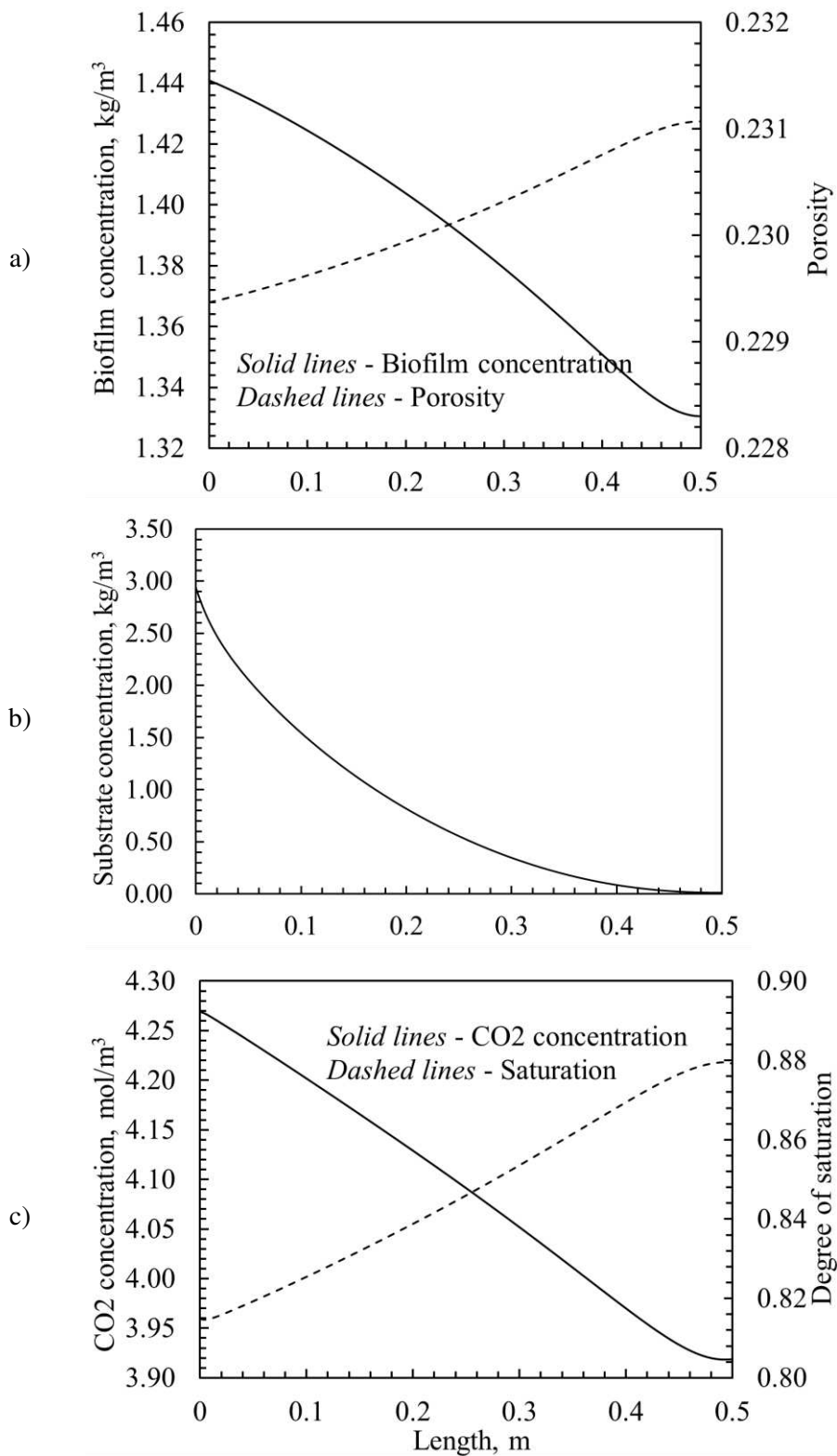


Figure 15 Profiles of a) biofilm and porosity, b) substrate, c) gas concentration and liquid saturation along the length of the sandstone sample during microbial fermentation. The profiles have been plotted after end of the simulation.

649

650 **6. Discussion and Conclusions**

651 In this paper, a new microbial model has been presented. Biomass transport, growth and decay processes
652 have been included within a coupled THCM framework. The THCM model, COMPASS, solves the
653 governing transport equations: suspended microbes in liquid phase, biofilms in solid phase,
654 multicomponent chemicals in liquid phase, multicomponent gas phase, liquid phase, heat and
655 mechanical deformation. The geochemical model, PHREEQC, estimates equilibrium and kinetic
656 reactions as well as redox behavior, changes in pH etc. The linked modelling platform enables a greater
657 range of applications involving fluids, chemicals, microbes and heat flow together with geochemical/
658 bio-geochemical reactions and deformation processes to be studied. In addition the multicomponent
659 feature of the model allows inter-community and intra-community microbial interactions to be
660 investigated.

661

662 Verification exercises demonstrated accurate implementations of the microbial processes in the model.
663 The model has been tested against the results of a laboratory experiment obtained from the literatures.
664 It is evident from the results that the model can predict qualitatively and quantitatively the effects of
665 microbial activities (*i.e.* net biofilm accumulation) on porous media properties (*i.e.* porosity,
666 permeability). Please note that the model is only partially evaluated at this stage. For full validation/
667 evaluation, relevant and comprehensive experimental data of microbial processes under multiphase
668 flow and reaction conditions are essential. However such information is scarcely available in the
669 literature.

670

671 To demonstrate the capabilities of the model, four sets of application are presented. These are; i) biofilm
672 growth at various gas injection rates, ii) effect of pH on microbial growth, iii) microbial respiration
673 under two-phase flow and iv) microbial fermentation and production of a gas phase. The results show
674 that in unsaturated conditions the extent of biofilm growth largely depends on the hydraulic properties
675 of the medium, if the growth is not limited by substrates or electron acceptors. If gas pressure is
676 relatively large and desaturates the medium then growth is restricted to the residual water volume.
677 Sufficient amount of liquid phase is essential for nutrient transport and biofilm development. Usage of
678 biofilms to enhance the barrier performances of a subsurface reservoir (*i.e.* carbon storage facility) or
679 caprocks might be less effective in such circumstances. To avoid that, media with higher water holding
680 capacity or lower gas injection (from injection-wells) and release (of sequestered gas from storage
681 formations) rates; together with faster growing biofilms could be preferred. The influence of
682 geochemical condition on biofilm growth has been modelled by varying the porewater pH (*i.e.*
683 dissolving CO₂ gas in the sandstone porewater). The results indicate that the growth is favoured by
684 higher pH values and is significantly retarded at lower pH. The capabilities of the model to simulate
685 microbial respiration under a coupled multiphase flow and microbial fermentation have been
686 demonstrated. The results suggest that respiration in two-phase flow is not only influenced by substrate
687 and oxidizer concentration but also by the gas concentration in the system. The simulated results of

688 microbial fermentation show that formation of a gas phase or change in gas phase composition can
 689 affect the coupled fluid flow processes in the system.

690

691 Parameters, such as, biofilm density, attachment and detachment rates, coefficient of shear loss, bio-
 692 geochemical rate parameters are (bacterial) species dependent and not widely available. In that regard,
 693 laboratory experiments should be carried out to obtain appropriate model parameters as well as relevant
 694 model information. For example, initial biofilm concentration is a key information for transient analysis.
 695 The onset of experimental studies and numerical models of biofilm growth is usually considered after
 696 the period of cell settlement and biofilm formation. The processes that take place during the settlement
 697 period are of significant importance, since they dictate the initial biofilm concentration in the medium.
 698 Further works will be carried out to address these issues.

699

700 Within the scope of this article, advanced capabilities of the model to study complex subsurface
 701 microbial processes have been demonstrated. However, the full extent of the model could not be utilised
 702 due to information limitations and/ essential simplifications. More complex and comprehensive
 703 scenarios of microbial processes and chemical reactions (*i.e.* equilibrium reactions, mineral
 704 precipitation/ dissolution kinetics etc.) involving wider extent of the geochemical model will be
 705 presented in future publications.

706

707 Appendix A

708 Table A Nomenclature

Symbol	Definition	Units
A, B, C	Coefficient matrices	
D_b^*, D_d^*	Hydrodynamic dispersion coefficient of suspended cells and dissolved chemicals in liquid phase	$m^2/s, m^2/s$
D_g^i, D_g^0	Effective, free flow diffusion coefficient of i^{th} gas species	$m^2/s, m^2/s$
D_d^0, D_d^i, D_d^h	Free flow chemical diffusion, effective chemical diffusion coefficient, mechanical dispersion in liquid	$m^2/s, m^2/s, m^2/s$
$[H^+]$	Concentration of hydrogen ion in liquid solution	mol/L
K_s', K_e'	Substrate, electron acceptor half-saturation constant	$kg/m^3, kg/m^3$
$K_{int}, K_{int,0}$	in-situ, original intrinsic permeability	m^2, m^2
N_g, N_d	Total number of gas, dissolved chemical components	
N_b^l, N_b^s	Total number of suspended cell, biofilm species	
P	Strain matrix	
R	Universal gas constant	J/K/mol
R_Ω	Residual error over the domain Ω	
S_l, S_g, S_r	Degree of liquid, gas, residual liquid saturation	$[-], [-], [-]$
S_s	Sink/source for liquid phase	kg/m^3
S_e	Effective saturation	$[-]$
T	Absolute temperature	$^\circ K$
Y, F	Yield coefficient of substrate, electron acceptor	$kg/kg, kg/kg$
b_s	Detachment rate due to liquid shear stress	s^{-1}

c_b^l	Suspended cell concentration <i>i.e.</i> the amount of suspended cell in the liquid phase	kg/m ³
c_b^s	Biofilm concentration <i>i.e.</i> the amount of attached biomass/biofilm in the whole porous media (soil)	kg/m ³
c_d^i	Concentration of the i^{th} chemical species in liquid	kg/m ³
c_d^s, c_d^e	Substrate, electron acceptor concentration in the liquid phase	kg/m ³ , kg/m ³
c_g^i	Concentration of the i^{th} species in the gas phase or air	mol/m ³
$c_c, c_-^b,$ k_+	Biocide decay parameters Substrate utilisation rate	[-], s ⁻¹ s ⁻¹
k_-, k_-^e, k_-^b	Combined, endogenous, biocide decay rate	s ⁻¹ , s ⁻¹ , s ⁻¹
k_{pH}	pH dependent growth rate	s ⁻¹
k_0^p, K_1^p	specific growth rate, ionisation constant	s ⁻¹ , mol/m ³
k_a, k_d	Rate constants for attachment, detachment of cells to, from biofilm	s ⁻¹ , s ⁻¹
k_{rl}, k_{rg}	Liquid, gas phase relative permeability	[-], [-]
k_τ	Specific shear loss coefficient	Pa ⁻¹ s ⁻¹
n_0, n	Initial unaffected, active porosity	[-], [-]
s_b^l	Sink/source for a suspended cell in liquid	kg/m ³
s_b^s	Sink/source for a biofilm in soil	kg/m ³
s_d^i	Sink/source for the i^{th} chemical in liquid	kg/m ³
s_g^i	Sink/source for the i^{th} gas component	mol/m ³
s, h	Suction, suction head	Pa, m
t	Time	s
u_l, u_g	Porewater, total poregas pressure	Pa, Pa
u	Displacement	m
v_l, v_g	Velocity of liquid, gas phase	m/s, m/s
α_L	Longitudinal dispersion coefficient	m
α, m, β	Curve fitting parameters of van Genuchten model	m ⁻¹ , [-], [-]
$\theta_l, \theta_g, \theta_b$	Volumetric liquid, gas, biofilm content	m ³ /m ³ , m ³ /m ³ , m ³ /m ³
μ_l, μ_g	Viscosity of liquid, gas	Pa s, Pa s
ρ_b^s	Biofilm mass density <i>i.e.</i> the amount of dry biomass per unit wet volume of the biofilm	kg/m ³
ρ_l, γ_l	Liquid density, unit weight of water	kg/m ³ , N/m ³
τ	Shear stress	Pa
τ_l, τ_g	Liquid phase, gas phase tortuosity factor	[-], [-]
φ	Vector of primary/independent model variables	
∇	Gradient operator	m ⁻¹

709

710 Appendix B

711 The mathematical relationship to define the effect of pH on microbial growth is presented in Equation
712 (12). In Figure B, the growth rate, k_{pH} is plotted against pH for a different combination of the
713 equation parameter (k_0^p, K_1^p) values (Table B). The parameter values in A, B, C and D are chosen
714 arbitrarily but within the published range available in literatures.

715

716 **Table B** Parameter values

	k_0^p	K_1^p

A	1.0×10^{-5}	1.0×10^{-7}
B	5.0×10^{-5}	1.0×10^{-7}
C	1.0×10^{-5}	5.0×10^{-7}
D	1.0×10^{-4}	1.0×10^{-6}

717

718 The graphs show that the rate is mostly sensitive to the specific growth rate, k_0^p for the selected
719 parameter values.

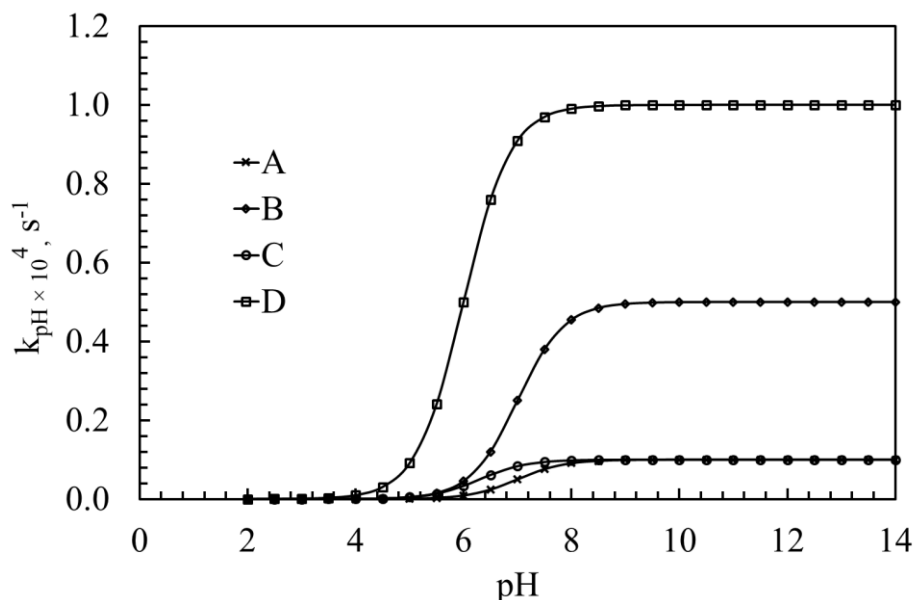


Figure B Sensitivity of the parameters on pH-dependent growth rate (k_{pH}) for various pH values.

720

721 Acknowledgement

722 Funding to support this research was provided by Welsh Government and HEFCW through Ser Cymru
723 National Research Network for Low Carbon, Energy and the Environment (NRN-LCEE) via *Geo-*
724 *Carb-Cymru* Cluster.

725

726 References

- 727 Bakke R, (1986). "Biofilm detachment". PhD Thesis, Montana State University, USA.
- 728 Baveye P, Vandevivere P, deLozada D, (1992). "Comment on biofilm growth and the related changes
729 in the physical properties of a porous medium, 1, Experimental investigation, *Water Resources*
730 *Research*, Vol 28, pp1481-1482.
- 731 Bear J, Verruijt A, (1987). *Modeling Groundwater Flow and Pollution*. D. Redel Pub. Co., Dordrecht,
732 pp 414.
- 733 Bethke CM, (2008). "Geochemical and Biogeochemical Reaction Modeling". 2nd ed., Cambridge
734 University Press, New York.
- 735 Beyenal H, Chen SN, Lewandowski Z, (2003). "The double substrate growth kinetics of *Pseudomonas*
736 *aeruginosa*". *Enzyme and Microbial Technology*, Vol 32, pp 92-98.

737 Chen-Charpentier B, (1999). “Numerical simulation of biofilm growth in porous media”. *Journal of*
738 *Computational and Applied Mathematics*, Vol 103, Issue 1, pp 55–66.

739 Corapcioglu MY, Haridas A, (1984). “Transport and fate of microorganisms in porous media: A
740 theoretical investigation”. *Journal of hydrology*, Vol 72, pp 149-169.

741 Corapcioglu MY, Haridas A, (1985). “Microbial transport in soils and groundwater: A numerical
742 model”. *Advances in Water Resources*, Vol 8, pp 188-200.

743 Costanza-Robinson MS, Brusseau ML, (2006). “Gas phase dispersion in porous media”. *Gas Transport*
744 *in Porous Media*, HO C and Webb S (eds), Springer, Dordrecht, The Netherlands.

745 Cunningham AB, Characklis WG, Abedeen F, Crawford D, (1991). “Influence of biofilm accumulation
746 on porous media hydrodynamics”. *Environ Science and Technology*, Vol 25, Issue 7, pp 1305–
747 1311.

748 Cussler EL, (1997). “Diffusion Mass Transfer in Fluid Systems”. 2nd ed., Cambridge University Press,
749 Cambridge.

750 Dixon M, Webb EC, (1979). “Enzymes”. Longman, London.

751 Douglas J, Jones BF, (1963). “On Predictor-Corrector Methods for Nonlinear Parabolic Differential
752 Equations”. *Journal of the Society for Industrial and Applied Mathematics*, Vol 11, Issue 1, pp
753 195-204.

754 Ebigbo A, Helmig R, Cunningham AB, Class H, Gerlach R, (2010). “Modelling biofilm growth in the
755 presence of carbon dioxide and water flow in the subsurface”. *Advances in Water Resources*, Vol
756 33 pp 762-781.

757 Efendiev M, (2013). “Evolution Equations Arising in the Modelling of Life Sciences”. *International*
758 *Series of Numerical Mathematics*, Vol 163, Springer, Basel, Heidelberg. Escher AR, (1986).
759 “Bacterial colonization of a smooth surface. An analysis with image analyzer”. PhD Thesis,
760 Montana State University, USA.

761 Escher AR, (1986). “Colonization of a Smooth Surface by *Pseudomonas aeruginosa*: image analysis
762 method”. PhD thesis, Montana State University, Bozeman, Montana, USA.

763 Fredlund DG, Rahardjo H, (1993). “Soil Mechanics for Unsaturated Soils”. John Wiley & Sons, Inc,
764 New York.

765 Gargiulo G, Bradford S, Simunek J, Ustohal P, Vereecken H, Klumpp E, (2007). “Bacteria transport
766 and deposition under unsaturated conditions: the role of the matrix grain size and the bacteria
767 surface protein”. *Journal of Contaminant Hydrology*, Vol 92, Issue (3–4), pp 255–273.

768 Gelhar LW, Welty C, Rehfeldt KR, (1992). “A critical review of data on field-scale dispersion in
769 aquifers”. *Water Resources Research*, Vol 28, Issue 7, pp 1955-1974.

770 Ginn TR, Wood BD, Nelson KE, Scheibe TD, Murphy EM, Clement TP, (2002). “Processes in
771 microbial transport in the natural subsurface”. *Advances in Water Resources*, Vol 25, pp 1017-
772 1042.

773 Hošťacká A, Čížnár I, Štefkovičová M, (2010). “Temperature and pH Affect the Production of Bacterial
774 Biofilm”. *Folia Microbiol*, Vol 55, Issue 1, pp 75-78.

775 Ibragimova SI, Nerova NM, Rabotnova IL, (1969). “Kinetics of growth inhibition in *Propionibac*
776 *shermanii* by hydrogen and hydroxyl ions”. *Microbiol*, Vol 38, pp 799-802.

777 Kim D, Chung S, Lee S, Choi J, (2012). “Relation of microbial biomass to counting units for
778 *Pseudomonas aeruginosa*”. *African Journal of Microbiology Research*, Vol 6, Issue 21, pp 4620-
779 4622.

780 Masum SA, Vardon PJ, Thomas HR, Chen Q, Nicholson D, (2012). “Multicomponent gas flow through
781 compacted clay buffer in a higher activity nuclear waste geological disposal facility”.
782 *Mineralogical Magazine*, Vol 76, Issue 8, pp 3337-3344.

783 Masum SA, (2012). “Modelling of reactive gas transport in unsaturated soil. A coupled thermo-hydro-
784 chemical-mechanical approach”. PhD thesis, Cardiff University, UK.

785 Maggi F, Porporato A, (2007). “Coupled moisture and microbial dynamics in unsaturated soils”. *Water*
786 *Resources Research*, Vol 43, W07444, doi:10.1029/2006WR005367.

787 Millington RJ, Quirk JM, (1961). “Permeability of porous solids”. *Transactions of Faraday Society*,
788 Vol 57, pp 1200–1207.

789 Mitchell AC, Phillips AJ, Hiebert R, Gerlach R, Spangler LH, Cunningham AB, (2009). “Biofilm
790 enhanced geologic sequestration of supercritical CO₂”. *International Journal of Greenhouse Gas*
791 *Control*, Vol 3, issue 1, pp 90-99.

792 Mostafa M, van Geel PJ, (2007). “Conceptual models and simulations for biological clogging in
793 unsaturated soils”. *Vadose Zone Journal*, Vol 6, Issue 1, pp 175–185.

794 Murphy EM, Ginn TR, (2000). “Modelling microbial processes in porous media”. *Hydrogeology*
795 *Journal*, Vol 8, pp 142-158.

796 Or D, Smets BF, Wraith JM, Dechesne A, Friedman SP, (2007). “Physical constraints affecting bacterial
797 habitats and activity in unsaturated porous media – a review”. *Advances in Water Resources*, Vol
798 30, pp 1505-1527.

799 Parker JC, Lenhard RJ, Kuppusamy T, (1987). “A Parametric Model for Constitutive Properties
800 Governing Multiphase Flow in Porous Media”. *Water Resources Research* 23, No. 4, pp. 618–
801 624.

802 Parkhurst DL, Appelo CAJ, (1999). “User’s Guide to PHREEQC (Version 2)”. Water Resource
803 Investigation Report, 99-4259. United States Geological Survey, Reston, VA.

804 Peyton BM, (1995). “Effects of shear stress and substrate loading rate on *Pseudomonas aeruginosa*
805 biofilm thickness and density”. *Water Research*, Vol 30, Issue 1, pp 29-36.

806 Pickens JF, Gilham RW, (1980). “Finite element analysis of solute transport under hysteresis
807 unsaturated flow conditions”. *Water Resources Research*, Vol 16, pp 1071-1078.

808 Postigo MA, Katz M, (1987). “Solubility and Thermodynamics of Carbon Dioxide in Aqueous Ethanol
809 Solutions”. *Journal of Solution Chemistry*, Vol 16, Issue 12.

810 Rittmann BE, McCarty PL, (1980). "Model of steady-state-biofilm kinetics". *Biotechnology and*
811 *Bioengineering*, Vol 22, pp 2343-2357.

812 Rittmann BE, (1982). "The effect of shear stress on biofilm loss rate". *Biotechnology and*
813 *Bioengineering*, Vol XXIV.

814 Rittmann BE, (1993). "The significance of biofilms in porous media". *Water Resources Research*, Vol
815 29, pp 2195–2202.

816 Rockhold ML, Yarwood RR, Selker JS, (2004). "Coupled microbial and transport processes in soils".
817 *Vadose Zone Journal*, Vol 3, Issue 2, pp 368–383.

818 Rosenzweig R, Furman A, Shavit U, (2013). "A channel network model as a framework for
819 characterizing variably saturated flow in biofilm-affected soils". *Vadose Zone Journal*, Vol 12,
820 Issue 2.

821 Rosenzweig R, Furman A, Dosoretz C, Shavit U, (2014). "Modelling biofilm dynamics and hydraulic
822 properties in variably saturated soils using a channel network model". *Water Resources*
823 *Research*, Vol 50, pp 5678–5697, doi:10.1002/2013WR015211.

824 Rousk J, Brookes PC, Bååth E, (2009). "Contrasting Soil pH Effects on Fungal and Bacterial Growth
825 Suggest Functional Redundancy in Carbon Mineralization ". *Applied and Environmental*
826 *Microbiology*, Vol 75, Issue 6, pp 1589-1596.

827 Schaefer A, Ustohal P, Harms H, Stauffer F, Dracos T, Zehnder AJB, (1998). "Transport of bacteria in
828 unsaturated porous media". *Journal of Contaminant Hydrology*, Vol 33, Issue (1–2), pp149–169.

829 Sedighi M, Thomas HR, Masum SA, Vardon PJ, Nicholson D, Chen Q, (2015). "Geochemical
830 modelling of hydrogen gas migration in an unsaturated bentonite buffer". Geological Society,
831 London, Special Publications, Vol 415, pp 189-201.

832 Seetharam SC, (2003). "An investigation of the thermo/hydro/chemical/mechanical behaviour of
833 unsaturated soils". PhD Thesis, Cardiff University, UK.

834 Seetharam SC, Thomas HR, Cleall PJ, (2007). "Coupled thermo-hydro-chemical-mechanical model for
835 unsaturated soils-Numerical algorithm". *International Journal of Numerical Methods in*
836 *Engineering*, Vol 70, pp 1480–1511.

837 Segel IH, (1975). "Enzyme kinetics: behavior and analysis of rapid equilibrium and steady-state enzyme
838 systems". Wiley-Interscience, New York.

839 Seki K, Miyazaki T, Nakano M, (1998). "Effects of microorganisms on hydraulic conductivity decrease
840 in infiltration". *European Journal of Soil Science*, Vol 49, Issue 2, pp 231–236.

841 Seki K, Miyazaki T, (2001). "A mathematical model for biological clogging of uniform porous media".
842 *Water Resources Research*, Vol 37, Issue 12, pp 2995–2999.

843 Sander R, (2015). "Compilation of Henry's law constants (version 4.0) for water as solvent".
844 *Atmospheric Chemistry and Physics*, Vol 15, pp 4399-4981.

845 Somerton WH, Söylemezoğlu IM, Dudley RC, (1975). "Effects of Stress on Permeability of Coal".
846 *International Journal of Rock Mechanics and Mining Sciences & Geomechanics Abstracts*, Vol
847 12, Issue 5-6, pp 129-145.

848 Tan Y, Wang Z, Marshall KC, (1998). "Modelling pH Effects on Microbial Growth: A Statistical
849 Thermodynamic Approach". *Biotechnology and Bioengineering*, Vol 59, pp 724-731.

850 Tang IC, Okos MR, Yang ST, (1989). "Effects of pH and acetic acid on homoacetic fermentation of
851 lactate by *Clostridium formicoaceticum*". *Biotechnology and Bioengineering*, Vol 34, pp 1063-
852 1074.

853 Taylor R, Krishna R, (1993). "Multicomponent Mass Transfer". John Wiley & Sons, Inc, New York.

854 Taylor SW, Milly PCD, Jaffe PR, (1990). "Biofilm growth and the related changes in the physical
855 properties of a porous medium 2. Permeability". *Water Resources Research*, Vol 26, Issue 9, pp
856 2161-2169.

857 Taylor SW, Jaffe PR, (1990a). "Biofilm growth and the related changes in the physical properties of a
858 porous medium 1. Experimental investigation". *Water Resources Research*, Vol 26, Issue 9, pp
859 2153-2159.

860 Taylor SW, Jaffe PR, (1990b) "Biofilm growth and the related changes in the physical properties of a
861 porous medium 3. Dispersivity and model verification". *Water Resources Research*, Vol 26,
862 Issue 9, pp 2171-2180.

863 Taylor SW, Jaffé PR, (1990c). "Substrate and biomass transport in a porous medium". *Water Resources
864 Research*, Vol 26, Issue 9, pp 2181–2194.

865 Thomas HR, He Y, (1998). "Modelling the behaviour of unsaturated soil using an elasto plastic
866 constitutive relationship". *Géotechnique*, Vol 48, Issue 5, pp 589–603.

867 Thullner M, Baveye P, (2008). "Computational pore network modelling of the influence of biofilm
868 permeability on bioclogging in porous media". *Biotechnology and Bioengineering*, Vol 99, Issue
869 6, pp 1337–1351.

870 Trulear MG, Characklis WG, (1980). "Dynamics of biofilm processes". Paper presented at the 53rd
871 Annual Conference of the Water Pollution Control Federation, Las Vegas, USA.

872 Vandevivere P, Baveye P, (1992a). "Saturated hydraulic conductivity reduction caused by aerobic
873 bacteria in sand columns". *Journal of Soil Science Society of America*, Vol 56, pp 1-13.

874 Vandevivere P, Baveye P, (1992b). "Effect of bacterial extracellular polymers on the saturated
875 hydraulic conductivity of sand columns". *Applied Environmental Microbiology*, Vol 58, pp 1690-
876 1698.

877 van Genuchten MTh, (1980). "A closed-form equation for predicting the hydraulic conductivity of
878 unsaturated soils". *Soil science society of America journal*, Vol 44, Issue 5, pp 892-898.

879 Wwwwbr.cr.usgs.gov. (2017). Attachment B--Description of Database Files and Listing. [online]
880 Available at: https://wwwbr.cr.usgs.gov/projects/GWC_coupled/phreeqc/html/final-90.html
881 [Accessed 21 Apr. 2017].

- 882 Yarwood RR, Rockhold ML, Niemet MR, Selker JS, Bottomley PJ, (2006). “Impact of microbial
883 growth on water flow and solute transport in unsaturated porous media”. *Water Resources*
884 *Research*, Vol 42, W10405.
- 885 Zhang J, Davis TA, Matthews MA, Drews MJ, LaBerge M, An YH, (2006). “Sterilization using high-
886 pressure carbon dioxide”. *Journal of Supercritical Fluids*, Vol 38, pp 354–372.